The Astrophysical Journal, 746:48 (15pp), 2012 February 10 doi:10.1088/0004-637X/746/1/48

WHAT IS THE MOST PROMISING ELECTROMAGNETIC COUNTERPART OF A NEUTRON STAR BINARY MERGER?

B. D. Metzger[1,3] and E. Berger[2]
[1] Department of Astrophysical Sciences, Peyton Hall, Princeton University, Princeton, NJ 08544, USA
[2] Harvard-Smithsonian Center for Astrophysics, 60 Garden Street, Cambridge, MA 02138, USA
Received 2011 August 30; accepted 2011 November 10; published 2012 January 24

ABSTRACT

The final inspiral of double neutron star and neutron-star–black-hole binaries are likely to be detected by advanced networks of ground-based gravitational wave (GW) interferometers. Maximizing the science returns from such a discovery will require the identification of an electromagnetic counterpart. Here we critically evaluate and compare several possible counterparts, including short-duration gamma-ray bursts (SGRBs), "orphan" optical and radio afterglows, and day-long optical transients powered by the radioactive decay of heavy nuclei synthesized in the merger ejecta ("kilonovae"). We assess the promise of each counterpart in terms of four "Cardinal Virtues": detectability, high fraction, identifiability, and positional accuracy. Taking into account the search strategy for typical error regions of tens of square degrees, we conclude that SGRBs are the most useful to confirm the cosmic origin of a few GW events, and to test the association with neutron star mergers. However, for the more ambitious goal of localizing and obtaining redshifts for a large sample of GW events, kilonovae are instead preferred. Off-axis optical afterglows are detectable for at most tens of percent of events, while radio afterglows are promising only for energetic relativistic ejecta in a high-density medium. Our main recommendations are: (1) an all-sky gamma-ray satellite is essential for temporal coincidence detections, and for GW searches of gamma-ray-triggered events; (2) the Large Synoptic Survey Telescope should adopt a one-day cadence follow-up strategy, ideally with 0.5 hr per pointing to cover GW error regions; and (3) radio searches should focus on the relativistic case, which requires observations for a few months.

Key words: gamma-ray burst: general – gravitational waves – stars: neutron – surveys

Online-only material: color figures

1. INTRODUCTION

The first direct detection of gravitational waves (GWs) is anticipated within the decade once the ground-based interferometers LIGO[4] (Abramovici et al. 1992; Abbott et al. 2009) and Virgo[5] (Caron et al. 1999; Acernese et al. 2009) are upgraded to "advanced" sensitivity (hereafter ALIGO/Virgo). The Large Scale Cryogenic Gravitational Wave Telescope (LCGT; Kuroda & LCGT Collaboration 2010) is under construction in Japan and is anticipated to join ALIGO/Virgo by about 2018. The most promising astrophysical GW sources in the frequency range of these detectors are the inspiral and coalescence of compact object binaries with neutron star (NS) and/or black hole (BH) constituents. Although this accomplishment will stand on its own merits, optimizing the science returns from a GW detection will require the identification and study of coincident electromagnetic (EM) counterparts (e.g., Schutz 1986, 2002; Sylvestre 2003; Stubbs 2008; Phinney 2009; Stamatikos et al. 2009; Bloom et al. 2009). This is important for several reasons, including lifting degeneracies associated with the inferred binary parameters (Hughes & Holz 2003); reducing the signal-to-noise ratio (S/N) for a confident GW detection (Kochanek & Piran 1993; Dalal et al. 2006; Harry & Fairhurst 2011); and identifying the merger redshift, thereby setting the energy scale and allowing an independent measurement of the Hubble constant or other cosmological parameters (e.g., Krolak & Schutz 1987; Chernoff & Finn 1993; Holz & Hughes 2005; Deffayet & Menou 2007; Nissanke et al. 2010). The potential wealth of complementary information encoded in the EM signal is likewise essential to fully unraveling the astrophysical context of the event (Phinney 2009; Mandel & O'Shaughnessy 2010), for example, an association with specific stellar populations (e.g., Fong et al. 2010).

Motivated by the importance of EM detections, in this paper we address the critical question: *What is the most promising EM counterpart of a compact object binary merger?* The answer of course depends on the definition of "most promising." In our view, a promising counterpart should exhibit four Cardinal Virtues, namely, it should:

1. Be detectable with present or upcoming telescope facilities, provided a reasonable allocation of resources.
2. Accompany a high fraction of GW events.
3. Be unambiguously identifiable (a "smoking gun"), such that it can be distinguished from other astrophysical transients and confidently associated with a particular GW event.
4. Allow for a determination of ∼arcsecond sky positions.

Virtue 1 is necessary to ensure that effective EM searches indeed take place for a substantial number of GW triggers. Virtue 2 is important because a large number of events may be necessary to build up statistical samples, particularly if GW detections are rare; in this context, ALIGO/Virgo is predicted to detect NS–NS mergers at a rate ranging from ∼0.4 to ∼400 yr^{-1}, with a "best-bet" rate of ∼40 yr^{-1} (Abadie et al. 2010a; cf. Kopparapu et al. 2008), while the best-bet rate for detection of NS–BH mergers is ∼10 yr^{-1}. Virtue 3 is necessary to make the association with high confidence and hence to avoid contamination from more common transient sources (e.g., supernovae). Finally, Virtue 4 is essential to identifying the host galaxy as well as other relevant properties (e.g., association

[3] NASA Einstein Fellow.
[4] http://www.ligo.caltech.edu
[5] http://www.virgo.infn.it

with specific stellar populations). Because merger counterparts are predicted to be faint, obtaining a spectroscopic redshift is challenging (cf. Rowlinson et al. 2010), in which case spectroscopy of the host galaxy is the most promising means of obtaining the event redshift.

It is important to distinguish two general strategies for connecting EM and GW events. One approach is to search for a GW signal following an EM trigger, either in real time or at a post-processing stage (e.g., Finn et al. 1999; Mohanty et al. 2004). This is particularly promising for counterparts predicted to occur in temporal coincidence with the GW chirp, such as short-duration gamma-ray bursts (SGRBs). Unfortunately, most other promising counterparts (none of which have yet been independently identified) occur hours to months after coalescence.[6] Thus, the predicted arrival time of the GW signal will remain uncertain, in which case the additional sensitivity gained from this information is significantly reduced. For instance, if the time of merger is known only to within an uncertainty of $\sim$ hours (weeks), as we will show is the case for optical (radio) counterparts, then the number of trial GW templates that must be searched is larger by a factor $\sim 10^4$–10^6 than if the merger time is known to within seconds, as in the case of SGRBs.

A second approach, which is the primary focus of this paper, is EM follow-up of GW triggers. A potential advantage in this case is that counterpart searches are restricted to the nearby universe, as determined by the ALIGO/Virgo sensitivity range (redshift $z \lesssim 0.05$–0.1). On the other hand, the large error regions are a significant challenge, which are estimated to be tens of square degrees even for optimistic configurations of GW detectors (e.g., Gürsel & Tinto 1989; Fairhurst 2009; Wen & Chen 2010; Nissanke et al. 2011). Although it has been argued that this difficulty may be alleviated if the search is restricted to galaxies within 200 Mpc (Nuttall & Sutton 2010), we stress that the number of galaxies with $L \gtrsim 0.1\,L^*$ (typical of SGRB host galaxies; Berger 2009, 2011) within an expected GW error region is $\sim$400, large enough to negate this advantage for most search strategies. In principle the number of candidate galaxies could be reduced if the distance can be constrained from the GW signal; however, distance estimates for individual events are rather uncertain, especially at that low of S/Ns that will characterize most detections (Nissanke et al. 2010). Moreover, current galaxy catalogs are incomplete within the ALIGO/Virgo volume, especially at lower luminosities. Finally, some mergers may also occur outside of their host galaxies (Berger 2010; Kelley et al. 2010). Although restricting counterpart searches to nearby galaxies is unlikely to reduce the number of telescope pointings necessary in follow-up searches, it nevertheless can substantially reduce the effective sky region to be searched, thereby allowing for more effective vetoes of false positive events (Kulkarni & Kasliwal 2009).

At the present there are no optical or radio facilities that can provide all-sky coverage at a cadence and depth matched to the expected light curves of EM counterparts. As we show in this paper, even the Large Synoptic Survey Telescope (LSST), with a planned all-sky cadence of four days and a depth of $r \approx 24.7$ mag, is unlikely to effectively capture the range of expected EM counterparts. Thus, targeted follow-up of GW error regions is required, whether the aim is to detect optical or radio counterparts. Even with this approach, the follow-up observations will still require large field-of-view (FOV) telescopes to cover tens of square degrees; targeted observations of galaxies are unlikely to substantially reduce the large amount of time to scan the full error region.

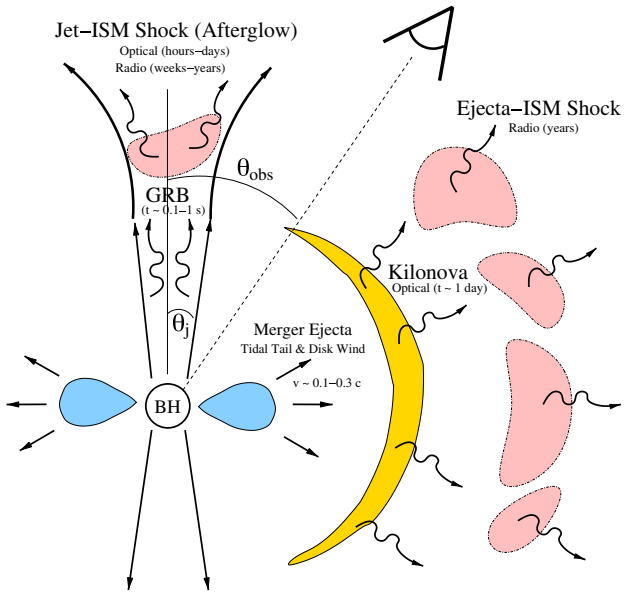

Figure 1. Summary of potential electromagnetic counterparts of NS–NS/NS–BH mergers discussed in this paper, as a function of the observer angle, $\theta_{\rm obs}$. Following the merger a centrifugally supported disk (blue) remains around the central compact object (usually a BH). Rapid accretion lasting $\lesssim$1 s powers a collimated relativistic jet, which produces a short-duration gamma-ray burst (Section 2). Due to relativistic beaming, the gamma-ray emission is restricted to observers with $\theta_{\rm obs} \lesssim \theta_j$, the half-opening angle of the jet. Non-thermal afterglow emission results from the interaction of the jet with the surrounding circumburst medium (pink). Optical afterglow emission is observable on timescales up to $\sim$ days–weeks by observers with viewing angles of $\theta_{\rm obs} \lesssim 2\theta_j$ (Section 3.1). Radio afterglow emission is observable from all viewing angles (isotropic) once the jet decelerates to mildly relativistic speeds on a timescale of weeks–months, and can also be produced on timescales of years from sub-relativistic ejecta (Section 3.2). Short-lived isotropic optical emission lasting $\sim$few days (kilonova; yellow) can also accompany the merger, powered by the radioactive decay of heavy elements synthesized in the ejecta (Section 4).

(A color version of this figure is available in the online journal.)

Our investigation of EM counterparts is organized as follows. We begin by comparing various types of EM counterparts, each illustrated by the schematic diagram in Figure 1. The first is an SGRB, powered by accretion following the merger (Section 2). Even if no SGRB is produced or detected, the merger may still be accompanied by relativistic ejecta, which will power non-thermal afterglow emission as it interacts with the surrounding medium. In Section 3 we explore the properties of such "orphan afterglows" from bursts with jets nearly aligned toward Earth (optical afterglows; Section 3.1) and for larger viewing angles (late radio afterglows; Section 3.2). We constrain our models using the existing observations of SGRB afterglows, coupled with off-axis afterglow models. We also provide a realistic assessment of the required observing time and achievable depths in the optical and radio bands. In Section 4 we consider isotropic optical transients powered by the radioactive decay of heavy elements synthesized in the ejecta (referred to here as "kilonovae," since their peak luminosities are predicted to be roughly one thousand times brighter than those of standard novae). In Section 5 we compare and contrast the potential counterparts in the context of our four Cardinal Virtues.

[6] Predicted EM counterparts that may instead *precede* the GW signal include emission powered by the magnetosphere of the NS (e.g., Hansen & Lyutikov 2001; McWilliams & Levin 2011; Lyutikov 2011a, 2011b), or cracking of the NS crust due to tidal interactions (e.g., Troja et al. 2010; Tsang et al. 2011), during the final inspiral. However, given the current uncertainties in these models, we do not discuss them further.

Although some of these counterparts have been discussed previously in the literature, we examine them together to better highlight their relative strengths and weaknesses. Drawing on the properties of the various counterparts, in Section 6 we make specific recommendations for optimizing the follow-up with γ-ray satellites, wide-field optical telescopes (Palomar Transient Factory (PTF), Pan-STARRS, LSST), and radio telescopes (Expanded Very Large Array (EVLA), ASKAP). We summarize our conclusions in Section 7.

2. SHORT-DURATION GAMMA-RAY BURSTS

The most commonly discussed EM counterpart of NS–NS/NS–BH mergers is an SGRB, powered by accretion onto the central compact object (e.g., Paczynski 1986; Eichler et al. 1989; Narayan et al. 1992; Rezzolla et al. 2011). The *Swift* satellite and rapid follow-up observations with ground-based telescopes have revolutionized our understanding of SGRBs by detecting and localizing a significant number of their afterglows for the first time (e.g., Berger et al. 2005; Fox et al. 2005; Hjorth et al. 2005; Bloom et al. 2006). This has enabled the discovery that SGRBs originate from more evolved stellar populations than those of long-duration GRBs, consistent with an origin associated with NS–NS mergers (Berger et al. 2005; Bloom et al. 2006; Leibler & Berger 2010; Berger 2011; Fong et al. 2011). The study of SGRB afterglows has also established a scale for the energy release and circumburst density that are lower than for long GRBs, with $E \lesssim 10^{51}$ erg and $n \lesssim 0.1$ cm^{-3} (Berger et al. 2005; Soderberg et al. 2006; Berger 2007). These observations have also provided evidence for collimation in at least one case (GRB 051221A), with a jet half-opening angle of $\theta_j \approx 0.12$ (Burrows et al. 2006; Soderberg et al. 2006), and upper or lower limits in additional cases (Fox et al. 2005; Grupe et al. 2006; Berger 2007), overall suggestive of wider opening angles than for long GRBs.

Despite this progress, it is not yet established that all SGRBs are uniquely associated with NS–NS/NS–BH mergers (e.g., Hurley et al. 2005; Metzger et al. 2008b), nor that all mergers lead to an energetic GRB. The energy of the GRB jet, for instance, may depend sensitively on the mass of the remnant accretion disk, which from numerical simulations appears to vary by orders of magnitude ($\sim 10^{-3}$ to 0.1 $M_\odot$), depending on the properties of the binary and the high-density equation of state (Ruffert et al. 1997; Janka et al. 1999; Lee 2001; Rosswog et al. 2003; Shibata & Taniguchi 2008; Duez et al. 2010; Chawla et al. 2010; Kyutoku et al. 2011).

Although SGRBs are bright, they occur relatively rarely within the range of ALIGO/Virgo. To illustrate this point, in Figure 2 we plot the cumulative rate at which SGRBs are currently detected above a redshift z, $\dot{N}_{\rm GRB,obs}(<z)$. This distribution includes 19 SGRBs with well-determined redshifts, obtained from host galaxy associations (e.g., Berger 2009). Since its launch in late 2004 *Swift* has detected SGRBs at a rate of ~ 10 yr^{-1}, of which $\sim 1/3$ have measured redshifts. Shown for comparison are the sensitivity ranges $D_{\rm r} \approx 1.5 \times 196[410] \approx 295[615]$ Mpc for detection of NS–NS[NS–BH] mergers by ALIGO/Virgo,[7] where the factor of ≈ 1.5 (included only in this section and Section 3.1; see Schutz 2011 and Equation (4)) accounts for the stronger GW signal from face-on mergers, which characterize the geometry of GRB jets (e.g., Kochanek & Piran 1993).

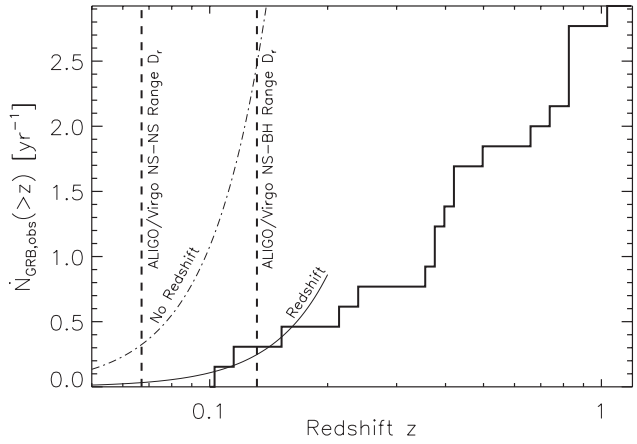

Figure 2. Cumulative detection rate of SGRBs with measured redshifts $< z$ (thick solid line), calculated using 19 (mostly *Swift*) SGRBs (e.g., Berger 2011). Dashed vertical lines mark the estimated sensitivity range of ALIGO/Virgo to NS–NS and NS–BH mergers, respectively, including a boost due to the face-on binary orientation. The thin solid line shows an approximate fit to $\dot{N}_{\rm GRB,obs}(< z)$ at low redshift. The dot-dashed line shows an estimate of the *total* SGRB detection rate (with or without redshift information) by an all-sky γ-ray telescope with a sensitivity similar to *Fermi*/GBM.

Figure 2 illustrates the striking fact that no SGRBs with known redshifts have yet occurred within the ALIGO/Virgo range for NS–NS mergers, while only two SGRBs (061201 and 080905A) have occurred within the NS–BH range. Though selection effects and low-number statistics undoubtedly distort the true redshift distribution from that shown in Figure 2, at low redshift the distribution should nevertheless scale as $\dot{N}_{\rm GRB,obs} \propto z^3$.[8] By fitting the lowest redshift bins to a distribution of this form, we find that $\lesssim 0.03(0.3)$ SGRBs per year are currently being localized by *Swift* within the ALIGO/Virgo range for NS–NS(NS–BH) mergers.[9] Thus, even assuming that *Swift* (or a mission with similar capabilities) operates simultaneously with ALIGO/Virgo, SGRBs are clearly not ideal counterparts to localize a large number of mergers. Obtaining a single GW redshift in this fashion could require a decade of observations.

Localization is of course only one desirable virtue of an EM counterpart. Due to the short duration of both SGRBs and the GW signal, and the short expected delay ($\lesssim$seconds) between them, a time coincidence between these events is sufficient to enable a statistically confident association. Even if the redshift cannot be obtained, a coincident detection will still confirm the astrophysical nature of the GW signal, prove the connection between SGRBs and NS–NS/NS–BH mergers, and allow studies of the dependence of the binary inclination on the properties of the GRB jet (e.g., Kochanek & Piran 1993). Coincidence searches for GW bursts using the time and sky coordinates of detected SGRBs were already conducted during

[7] Throughout this paper we adopt the fiducial values for $D_{\rm r} \approx 200$ Mpc from Abadie et al. (2010a), who define detections as events with S/N of 8 in a single detector, assuming NS/BH masses of 1.4/10 $M_\odot$. This choice is conservative because for a network of N detectors, the sensitivity range at fixed S/N increases $D_{\rm r} \propto N^{1/2}$. On the other hand, the real detection range of a network depends on the data quality (e.g., Gaussianity and stationarity) and detection pipeline. Once a value for $D_{\rm r}$ is chosen, all of the results presented in this paper may be rescaled accordingly.

[8] In general interpolating the observed SGRB redshift distribution depends on the luminosity function. Here we have assumed that SGRBs are well approximated as standard candles (see O'Shaughnessy et al. 2008 for a more general discussion).

[9] The sensitivity range for a GW detection may be increased somewhat if the search is restricted to the time interval and sky position of the SGRB in the case of a γ-ray-triggered search (Kochanek & Piran 1993), but this does not alter our conclusion that SGRBs are a rare occurrence in the range of ALIGO/Virgo.

previous LIGO/Virgo Science Runs (e.g., Abadie et al. 2010b; Abbott et al. 2010)

To estimate how long ALIGO/Virgo must operate before a connection between SGRBs and NS–NS/NS–BH mergers can be tested, we also plot in Figure 2 an estimate of the low-redshift distribution, but including *all* detectable SGRBs (with or without redshift information), which we estimate by multiplying the "with redshift" distribution by a factor ≈10. This factor accounts for the higher rate, ∼40 yr^{-1}, that *Fermi*'s Gamma-Ray Burst Monitor (GBM) detects SGRBs, compared to the rate with redshift from *Swift* (correcting also for the GBM FOV, which covers only ∼60% of the sky). This estimate illustrates that a few *Fermi* bursts over the past few years probably occurred within the ALIGO/Virgo volume. Thus, an all-sky γ-ray monitor with a sensitivity similar to *Fermi*/GBM could test whether SGRBs originate from NS–NS/NS–BH mergers within just a few years after ALIGO/Virgo reaches full sensitivity, even if it does not lead to a significant improvement in the sky localizations.

One issue raised by the above analysis is that the observed SGRB rate within the ALIGO/Virgo volume, even when corrected for partial sky coverage, is much lower than the best-bet NS–NS merger rate of ∼40 yr^{-1}. Nakar et al. (2006) estimate that the local volumetric SGRB rate is $\gtrsim$10 Gpc^{-3} yr^{-1}, which corresponds to an all-sky rate of $\dot{N}_{\rm GRB,all-sky} \sim 0.3$ yr^{-1} at a distance of $\lesssim D_{\rm r,NS-NS} \approx 200$ Mpc (cf. Guetta & Piran 2005), consistent with our estimates in Figure 2 and still two orders of magnitude below ∼40 yr^{-1}. Reconciling this remaining discrepancy requires either that the true merger rate is much lower than the best-bet rate; that all mergers are not accompanied by a bright SGRB; or that the γ-ray emission is considerably beamed (e.g., Rosswog & Ramirez-Ruiz 2002; Aloy et al. 2005).

Expanding on this final possibility, if the typical SGRB jet has a half-opening angle $\theta_j \lesssim \pi/2$, then only a fraction $f_{b,\gamma} \approx 1-\cos\theta_j \approx \theta_j^2/2 \ll 1$ of viewers with observing angles $\theta_{\rm obs} \lesssim \theta_j$ will detect a bright SGRB. For all other observers (the majority of cases) the prompt emission is much dimmer due to relativistic beaming. Reconciling the "observed" and best-bet rate by beaming alone thus requires $f_{b,\gamma} \sim 0.01$, or $\theta_j \sim 0.12$, similar to the opening angle inferred for GRB 051221A (Burrows et al. 2006; Soderberg et al. 2006).

A mystery associated with SGRBs is that ∼1/4–1/2 are followed by variable X-ray emission with a fluence comparable to or in excess of the initial burst (e.g., Norris & Bonnell 2006; Perley et al. 2009). Although the origin of this extended emission is still debated, one explanation is that it results from ongoing energy output from a highly magnetized neutron star, which survives the NS–NS merger (Metzger et al. 2008b; Bucciantini et al. 2012). Regardless of its origin, if some mergers are indeed accompanied by extended X-ray emission, this provides an additional potential EM counterpart, especially if the X-ray emission is more isotropic than the SGRB itself (as predicted by several models: MacFadyen et al. 2005; Metzger et al. 2008b; Barkov & Pozanenko 2011; Bucciantini et al. 2012). Considering alternative prompt counterparts is germane because the lifetimes of *Swift* and *Fermi* are uncertain, while the next generation of proposed high-energy transient satellites (e.g., *JANUS*, Burrows et al. 2011; *Lobster,* Gorenstein 2011; and *SVOM*, Götz et al. 2009) are most sensitive at soft X-ray (rather than γ-ray) energies, which could reduce their sensitivity to detecting the prompt SGRB phase. The difficulty of relying on this extended X-ray signal is twofold: (1) separating the off-axis extended emission from soft long GRBs in individual cases, and (2) these events represent only a fraction of all SGRBs.

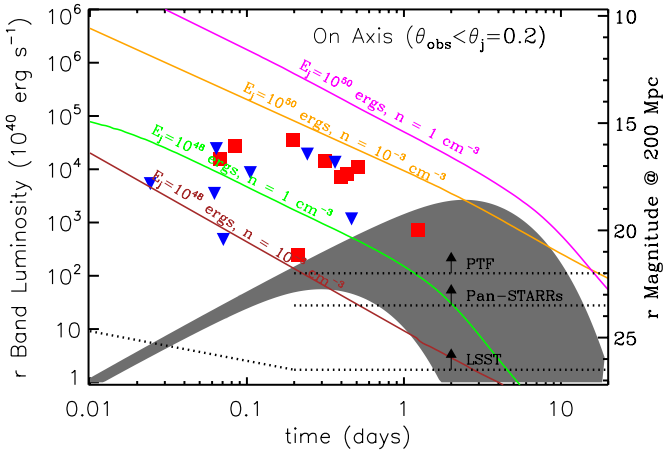

Figure 3. Optical rest-frame luminosity of existing SGRB afterglows (detections: red squares; upper limits: blue triangles; Berger 2010; Fong et al. 2011). Solid lines are afterglow models from van Eerten & MacFadyen (2011; see also van Eerten et al. 2010), calculated for on-axis observers ($\theta_{\rm obs} = \theta_{\rm j} = 0.2$) for a range of jet energies ($E_{\rm j}$) and circumburst densities (n). The existing afterglows define an upper bound on a figure of merit, ${\rm FOM}_{\rm opt,on} \equiv E_{j,50}^{4/3} n_0^{1/2} \lesssim 0.1$. Also shown are a range of plausible kilonova models (gray shading). The 5σ limiting magnitudes of various wide-field telescopes are marked by dashed lines; for PTF and Pan-STARRS we assume a maximum of 0.5 hr per pointing to cover a typical GW error region with a one-day cadence, while for LSST we show both the normal survey depth and the depth for 0.5 hr exposures.

(A color version of this figure is available in the online journal.)

3. AFTERGLOWS

Even in the absence of an SGRB, an orphan afterglow (e.g., van Eerten et al. 2010) may provide a bright EM link to a GW trigger (e.g., Coward et al. 2011; Nakar & Piran 2011). The orphan afterglow can be on-axis if the γ-ray emission was missed due to incomplete sky coverage by γ-ray satellites, or it can be off-axis if the relativistic jet was initially pointed away from our line of sight. For off-axis observers the afterglow emission peaks at a later time and at a lower brightness level than for on-axis observers, making the detection of a counterpart more challenging. However, a higher fraction of events, $\propto \theta_{\rm obs}^2$, occur at larger angles, with the total fraction of detectable counterparts depending on the largest viewing angle at which emission is still detectable. On a timescale of ∼days after the merger, the afterglow emission is still partially beamed and peaks at optical wavelengths (Section 3.1). At later times, weeks–months, the emission is mostly isotropic and peaks at radio wavelengths, once the jet decelerated to mildly relativistic velocities, $\beta \ll 1$ (Section 3.2).

3.1. Optical Afterglow

To gain insight into the afterglow emission that may accompany a merger event (on- or off-axis), we use existing observations of SGRB optical afterglows discovered in rapid follow-up observations. Figure 3 shows optical detections and upper limits from the compilation of Berger (2010) and Fong et al. (2011), expressed in luminosity and in apparent magnitude for a source at a distance of 200 Mpc. Shown for comparison are on-axis SGRB afterglow models with $\theta_{\rm obs} \approx \theta_j$ from van Eerten & MacFadyen (2011)[10] (see also van Eerten et al. 2010) that span the range of detected afterglows. Also shown are the sensitivity limits of existing and planned wide-field survey telescopes (PTF,

[10] http://cosmo.nyu.edu/afterglowlibrary/

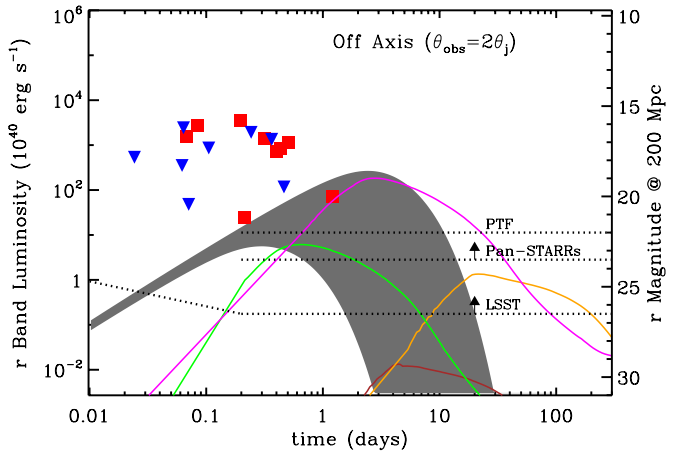

Figure 4. Same as Figure 3 but for off-axis observers with $\theta_{obs} \approx 2\theta_j$. The kilonova emission (gray shading) is isotropic and hence remains unchanged for both on- and off-axis observers. The range of existing SGRB optical afterglows, covered by the yellow, green, and brown lines, indicates that observations with LSST are essential.

(A color version of this figure is available in the online journal.)

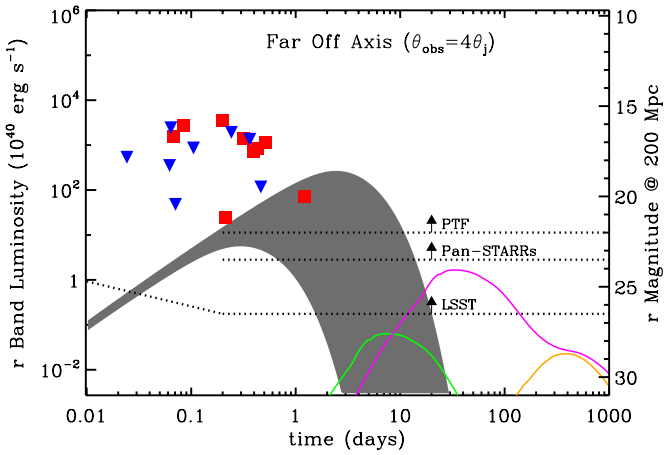

Figure 5. Same as Figure 4 but for off-axis observers with $\theta_{obs} \approx 4\theta_j$. The kilonova emission (gray shading) is isotropic and hence remains unchanged for both on- and off-axis observers. The range of existing SGRB optical afterglows, covered by the yellow, green, and brown lines (well below the limit of the plot), indicates that no existing or future telescope will be able to detect optical emission at such large off-axis angles.

(A color version of this figure is available in the online journal.)

Pan-STARRS, LSST), taking into account that about 10 pointings will be required to cover a typical GW error region, leading to at most 0.5 hr per pointing to cover the region in a single night; for LSST we also show the expected depth of the normal survey mode ($r \approx 24.7$ mag), which can cover a GW error region in only a few minutes. The expected maximum depth is about 22 mag for PTF, 23.5 mag for Pan-STARRS, and 26.5 mag for LSST. We note that the trade-off between limiting magnitude and localization area (A) is simply $\Delta m \approx -2.5\log(A^{1/2})$ such that for a best-case scenario of $A \sim$ few deg^2, these telescopes can achieve a greater depth by about 1.2 mag in a single night.

Figure 3 demonstrates that for a typical jet half-opening angle of $\theta_j = 0.2$, afterglow models with jet energies of $E_j \approx 10^{48}$–10^{50} erg and circumburst densities of $n \approx 10^{-3}$ to 1 cm^{-3} are consistent with the range of observed optical luminosities. We can define a figure of merit for the combination of energy and density (e.g., Granot & Sari 2002), which based on the observed on-axis optical afterglow luminosities has an upper bound of

$$\mathrm{FOM}_{\mathrm{opt,on}} \equiv E_{j,50}^{4/3}\, n_0^{1/2} \lesssim 0.1 \qquad (1)$$

and a mean value for the detected sample of $\mathrm{FOM}_{\mathrm{opt,on}} \sim 0.01$; here $E_{j,50}$ is the jet energy in units of 10^{50} erg, n_0 is the circumburst density in units of cm^{-3}, and we assume a typical value of $p = 2.5$ for the electron power-law distribution. We note that the sample in Figure 3 represents all SGRBs with deep optical searches, and hence also a detected X-ray afterglow. Since $\sim$1/4 of SGRBs lack detected X-ray afterglows, and not all events with X-ray detections had deep follow-up optical searches, it is possible that some SGRB optical afterglows are dimmer than those in Figure 3, leading to an even lower mean value of $\mathrm{FOM}_{\mathrm{opt,on}}$ than inferred above. Nevertheless, we conclude that $\sim$1/2 of SGRBs within the range of ALIGO/Virgo (even those missed due to incomplete γ-ray sky coverage) should produce optical emission detectable by LSST for at least $\sim$10 days; the brightest events should be detectable for a few days even by less sensitive surveys such as PTF.

Using the range of energies and circumburst densities inferred for on-axis afterglows, we can now predict the appearance of off-axis light curves. Figure 4 shows the same range of models from Figure 3, but now for an observer angle of $\theta_{obs} = 2\theta_j$. For the parameters of existing SGRB afterglows, the peak flux at even larger viewing angles (e.g., $\theta_{obs} = 4\theta_j$; Figure 5) is too low to be detected even with LSST. For the range of applicable models, the off-axis light curves rise to maximum brightness on a timescale of $\sim$1–20 days, with a peak luminosity of $\sim 10^{38}$–10^{41} erg s^{-1}; this corresponds to a apparent brightness of $\gtrsim$23 mag at 200 Mpc. The models with $n = 10^{-3}$ cm^{-3} peak on a timescale about 7 times longer, and with a luminosity that is about 300 times lower, than those with $n = 1$ cm^{-3}. We also note that the off-axis afterglow light curves in the higher density cases are qualitatively similar to those of kilonovae, although the latter fade more rapidly after the peak and have a distinct color evolution (Section 4).

For the off-axis light curves we can define a separate figure of merit (cf. Equation (11) of Nakar & Piran 2011):

$$\mathrm{FOM}_{\mathrm{opt,off}} \equiv E_{j,50}\, n_0^{7/8}. \qquad (2)$$

We define detectable cases as those rising by at least an order of magnitude (2.5 mag) above the LSST maximal depth, corresponding to $\mathrm{FOM}_{\mathrm{opt,off}} \gtrsim 0.002$ (Figures 4 and 6). With the same criterion for the threshold, a shallow survey such as PTF will only detect events with $\mathrm{FOM}_{\mathrm{opt,off}} \sim 1$, beyond the range of existing on-axis SGRB afterglows. In Figure 6 we plot the detectable region in the E_j–n phase space for the maximal LSST depth and the LSST normal survey depth ($\mathrm{FOM}_{\mathrm{opt,off}} \gtrsim 0.01$). The allowed phase space is bounded by the on-axis figure of merit (Equation (1)), and we also introduce an upper density cutoff of $n \lesssim 1$ cm^{-3} as an optimistic density for a merger in the interstellar medium of a disk galaxy. Due to the different dependencies of $\mathrm{FOM}_{\mathrm{opt,on}}$ and $\mathrm{FOM}_{\mathrm{opt,off}}$ on E_j and n, these conditions define a triangular region of allowed phase space for detections of off-axis optical afterglows; in Section 3.2 we perform a similar calculation for off-axis radio afterglows to compare the relative E_j–n phase space that is probed by each band. Most importantly, we find that the tracks for existing SGRB afterglows cross the phase-space region covered by optical searches.

We explore the detectability of on- and off-axis optical afterglows more precisely with a Monte Carlo simulation to determine the fraction of GW events within 200 Mpc that would

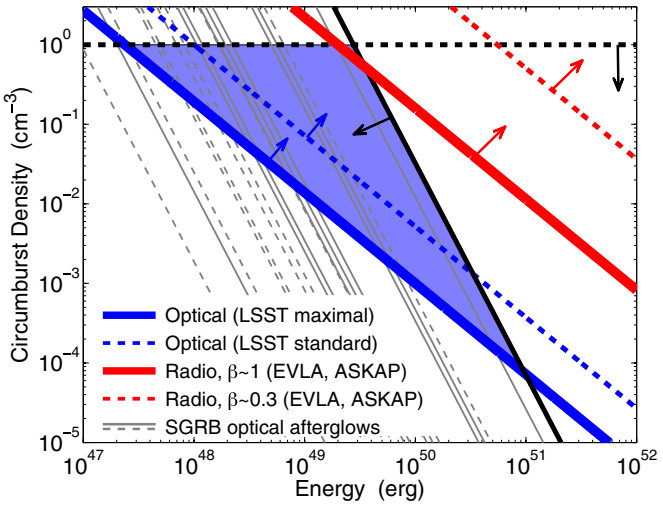

Figure 6. Phase space of energy and circumburst density that is accessible to off-axis afterglow searches in the optical (shaded blue) and radio (red). The solid and dashed blue lines mark the lower bounds for searches with a maximal LSST depth (26.5 mag) and the standard depth (24.7 mag). The dashed red line marks the lower bound for radio emission from ejecta with $\beta \sim 0.3$. The solid black line corresponds to the *upper* bound defined by existing SGRB optical afterglows ($\mathrm{FOM}_{\mathrm{opt,on}} \lesssim 0.1$; Equation (1)), while the black dashed line marks the expected upper bound on the density ($n = 1$ cm^{-3}) for mergers in the interstellar medium of a disk galaxy. Finally, the gray solid (dashed) lines mark the tracks for existing SGRB optical afterglow detections (limits) from Figure 3. The existing data suggest that radio detections are highly unlikely. On the other hand, the phase space accessible to optical searches is populated by at least some of the existing events.

(A color version of this figure is available in the online journal.)

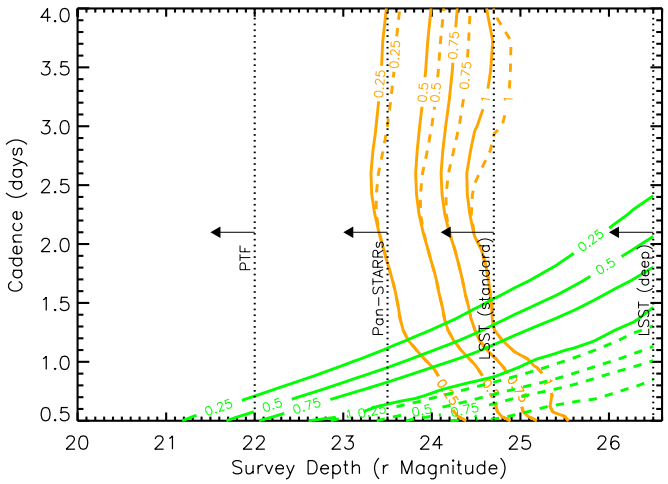

Figure 7. Fraction of off-axis optical afterglow events detected in three (solid line) or five (dashed line) epochs as a function of the depth and cadence of a search. The two models shown—$E_j = 10^{50}$ erg, $n = 10^{-3}$ cm^{-3} and $E_j = 10^{48}$ erg, $n = 1$ cm^{-3}—have the same colors as in Figure 3.

(A color version of this figure is available in the online journal.)

be detected by an optical survey with a given limiting magnitude and cadence. For targeted follow-up searches we use a one-day cadence with limiting magnitudes of 22 (PTF), 23.5 (Pan-STARRS), and 26.5 (LSST); we also include a one-day and four-day cadence with the standard LSST depth of 24.7 mag. The results, summarized in Table 2, show that if the jet energy and circumburst density are similar to those required to explain the on-axis SGRB data (Figure 3), then events with $\theta_{\mathrm{obs}} \lesssim 2\theta_j$ are sufficiently bright to be detected in at least three to five epochs, given a survey with a depth similar to the standard LSST survey (24.7 mag), but with a faster cadence of $\sim$1 day. Shallower searches are also capable of detecting energetic afterglows in a few epochs, but this may not be sufficient for a clear identification. By contrast, in most cases events viewed at larger angles ($\theta_{\mathrm{obs}} \gtrsim 2\theta_{\mathrm{j}}$) are not detectable, even near peak emission with LSST.

The same information is presented graphically in Figure 7 where we plot contours of detection fraction in three and five epochs as a function of depth and cadence. We find that in the case of $E_j \sim 10^{50}$ erg, the standard LSST cadence and depth are sufficient for multiple detections. However, for lower energies (which may be typical of most SGRBs), a faster cadence and greater depth ($\sim$26.5 mag) are required for multiple detections. To achieve a detection fraction of 50% in 3(5) epochs for the case of $\theta_{\mathrm{obs}} = 2\theta_j$ requires a depth of at least 23.5(26) mag for a one-day cadence.

Since detectable optical emission is limited to off-axis angles of $\lesssim 2\theta_j$, we estimate the corresponding fraction of GW events with potential optical afterglow detections as

$$f_{\mathrm{opt}} \approx \int_0^{2\bar{\theta}_{\mathrm{j}}} p_{\mathrm{det}} d\theta \approx 6.8\bar{\theta}_{\mathrm{j}}^2 + \mathcal{O}\left(\bar{\theta}_j^{\,4}\right), \qquad (3)$$

where $\bar{\theta}_{\mathrm{j}} \ll 1$ is the average opening angle, and

$$p_{\mathrm{det}}(\theta) \approx 0.152 \sin\theta (1 + 6\cos^2\theta + \cos^4\theta)^{3/2} \qquad (4)$$

is the detection probability of events with inclination angles between θ and $\theta + d\theta$ (e.g., Schutz 2011; their Equation (28)). As noted earlier, since this scenario is nearly face-on, f_{opt} is a factor $\sim$3.4 higher than the detection fraction $\approx 1 - \cos 2\theta_j \approx 2\bar{\theta_j}^2$ for isotropic emission.

Equation (3) shows that if the average opening angle is $\bar{\theta}_j \simeq 0.12$, which is the value inferred for GRB 051221A (Burrows et al. 2006; Soderberg et al. 2006), as well as the typical opening angle required to reconcile the observed SGRB rate with the best-bet NS–NS merger rate (Section 2), then up to $f_{\mathrm{opt}} \sim 0.1$ of GW events will be accompanied by potentially detectable optical afterglows. This result is consistent with the rate of a few afterglows per year inferred by Coward et al. (2011) for their assumed total ALIGO/Virgo merger rate of $\sim$135 yr^{-1}. On the other hand, if $\bar{\theta}_j$ is much larger, $\gtrsim$0.4 (e.g., as found for GRB 050724 by Grupe et al. 2006), then f_{opt} is of order unity, but the overall GW event rate may be lower than the best-bet ALIGO/Virgo rate.

Beyond considerations of depth and cadence, a unique optical identification of GW events also requires discrimination between off-axis afterglows and potential contaminants. We discuss this issue in Section 5.

3.2. Radio Afterglow

NS–NS/NS–BH mergers may also be accompanied by non-thermal radio afterglow emission, which can originate either from the ultra-relativistic jet (as in the case of the optical afterglow), or from more spherical, sub-relativistic ejecta (Nakar & Piran 2011; hereafter NP11). The latter includes matter ejected dynamically during the merger process ("tidal tails"), or in outflows from the accretion disk (see Figure 1). Adopting standard models for synchrotron emission from a relativistic shock, NP11 estimate that the peak radio brightness for these cases is

$$F_{\nu,\mathrm{p}} \approx 40\, E_{j,50}\, n_0^{7/8}\, \beta_{0.2}^{11/4}\, d_{L,200}^{-2}\, \nu_1^{-3/4} \ \mu\mathrm{Jy}, \qquad (5)$$

where $\beta_{0.2} = v_{\rm ej}/0.2c$, ν_1 is the observing frequency in GHz; and $d_L = 200 d_{L,200}$ Mpc is the luminosity distance, again normalized to the ALIGO/Virgo range for NS–NS mergers. Equation (5) also assumes characteristic values of $p = 2.5$ for the electron distribution power-law index, and $\epsilon_e = \epsilon_B = 0.1$ for the fractions of energy density imparted to relativistic electrons and magnetic fields, respectively. The radio emission peaks at the deceleration time

$$t_{\rm dec} \approx 2.6\, E_{j,50}^{1/3}\, n_0^{-1/3}\, \beta_{0.2}^{-5/3} \ \ {\rm yr}. \quad (6)$$

The peak brightness depends sensitively on both the properties of the ejecta (E and β) and on the circumburst density. As we discuss in detail below, the realistic detection threshold for a convincing detection with EVLA (even with ∼30 hr per epoch) is about 0.5 mJy. This requirement therefore defines a figure of merit for a radio detection of

$${\rm FOM}_{\rm rad} \equiv E_{j,50}\, n_0^{7/8}\, \beta^{11/4} \gtrsim 0.2. \quad (7)$$

With the exception of the velocity parameter, this figure of merit is identical to the case of off-axis optical afterglows in terms of the dependence on E_j and n.

For quasi-spherical ejecta, a characteristic mass of $M_{\rm ej} \sim 10^{-2}\, M_\odot$ in tidal tails or disk winds has an energy $E \approx M_{\rm ej} v_{\rm ej}^2/2 \sim 10^{50}$–$10^{51}$ erg for the expected range of velocities[11] $\beta \sim 0.1$–0.3. This results in at most ${\rm FOM}_{\rm rad} \approx 0.4\, n_0^{7/8}$, requiring $n_0 \gtrsim 1\ {\rm cm}^{-3}$ for a detection. For more typical densities of $\lesssim 0.1\ {\rm cm}^{-3}$ associated with SGRBs (Berger et al. 2005; Soderberg et al. 2006), the radio emission from quasi-spherical ejecta will be essentially undetectable unless the energy scale is much larger than $\sim 10^{51}$ erg (Figure 6).

Equations (5)–(7) can also be applied to the case of off-axis afterglow emission using $\beta \approx 1$ (Nakar & Piran 2011) along with values for the jet energy and circumburst density inferred from the optical afterglow data (${\rm FOM}_{\rm opt,on} \lesssim 0.1$; Equation (1)). In Figure 6 we plot the region of E–n phase space that is accessible to radio detections (${\rm FOM}_{\rm rad} \gtrsim 0.2$). As can be seen from the figure, none of the existing SGRB optical afterglow intersect this region, indicating that radio detections of off-axis afterglows are likely to be rare despite the overall isotropy of the signal.

We now address in detail the estimated minimum radio brightness necessary for a successful detection. Although faint radio emission is in principle detectable with a deep integration, a significant challenge is the small FOV of sensitive instruments such as the EVLA (≈0.4 deg^2 at 1 GHz), requiring ∼100–200 pointings to cover a typical GW error region of tens of square degrees. Targeting individual galaxies within the error region does not decrease the number of required pointings since there are ∼400 galaxies with $L \gtrsim 0.1\, L^*$ within a typical error region (to 200 Mpc). Even with only 10 minutes per pointing, ∼30 hr per epoch will be required to cover the full error region,[12] already a substantial allocation of EVLA time. Multiple epochs will be required over a span of weeks to years to detect the rise and decline of the radio light curve following a GW detection (Equation (6)), for a total of about ∼300 hr of EVLA time (i.e., to search the best-bet rate of ∼40 GW triggers per year will require essentially 100% of the EVLA time). Thus, a reasonable exposure time per pointing is $\lesssim$10 minutes, which at 1 GHz corresponds to a 5σ limit[13] of about 0.25 mJy. Since a convincing detection will require the brightness to rise to about twice the threshold, the minimum detectable peak flux is $F_{\nu,{\rm p}} \approx 0.5$ mJy. We note that the threshold may be even higher in the compact EVLA configurations (C and D) due to substantial source confusion imposed by the large synthesized beam size (12″–44″).

Observations at a higher frequency of 5 GHz can in principle provide better sensitivity (and reduce source confusion problems), but in reality will actually require even more observing time. This is mainly because the FOV at 5 GHz is sufficiently small (0.02 deg^2) that a more profitable strategy is to target the ∼400 galaxies with $L \gtrsim 0.1\, L^*$ within a typical GW error region. Even with only five minutes per pointing this will require about 40 hr per epoch, with a resulting 5σ limit of 0.1 mJy. A convincing detection will therefore require $F_{\nu,{\rm p}} \gtrsim 0.2$ mJy, which given a typical spectrum of $F_{\nu,{\rm p}} \propto \nu^{-0.75}$ is equivalent to a limit of $\gtrsim$0.7 mJy at 1 GHz, worse than the 1 GHz observing strategy, with even more time required per epoch.

Observations with future wide-field radio interferometers (e.g., ASKAP) will cover a typical GW error region with a few pointings, requiring only a few hours per epoch. However, these instruments suffer from poorer angular resolution compared to what is possible with EVLA (e.g., ASKAP with ∼10″ resolution). This will lead to significant source confusion at the required low flux density levels. More critically, radio emission from the host galaxy itself will present a challenge; at 200 Mpc a star formation rate of only 1 $M_\odot$ yr^{-1} corresponds to a 1 GHz flux density of about 0.6 mJy (Yun & Carilli 2002). At a resolution of 10″ (10 kpc at 200 Mpc), galaxies will generally appear as unresolved point sources and will prevent the detection of significantly fainter coincident radio counterparts. Thus, an instrument like ASKAP will cover a GW error region faster than the EVLA, but to a similar effective depth limited by source confusion.

A final complication with radio detections is the long time delay between a GW trigger and the peak of the putative radio signal, which could negate a robust association. For a subrelativistic counterpart ($\beta \sim 0.2$) with an optimistic density of $n \sim 1\ {\rm cm}^{-3}$, a detection requires $E \gtrsim 10^{51}$ erg (Equation (7)), and as a result $t_{\rm dec} \approx 6$ yr, requiring observations for over a decade. For the relativistic case ($\beta \approx 1$) with $n \sim 1\ {\rm cm}^{-3}$, the peak time corresponding to a detectable signal is $t_{\rm dec} \approx 0.1$ yr. The latter case will require a ∼one-week cadence to robustly sample the light curve, corresponding to about 15%–20% of the EVLA time (with ∼30 hr per epoch). The absence of a credible detection will require a ∼one-year cadence to search for a non-relativistic counterpart. Of course, with a multi-year timescale the probability of misidentification with an unrelated radio transient becomes larger.

Despite the various difficulties outlined above, a clear advantage of radio searches is the lower number of contaminating sources compared to the optical band. As discussed in NP11, confusion with active galactic nucleus (AGN) radio variability can be reduced by requiring an offset from the center of the host galaxy, although this may be difficult with an angular resolution of $\gtrsim$10″ (EVLA in its compact configurations and ASKAP). Similarly, while some normal Type Ib/c supernovae

[11] The ejecta mass and velocity may be higher in some NS–BH mergers (e.g., Rosswog 2005), especially those that merge on eccentric orbits in dense stellar clusters (e.g., Lee et al. 2010; Stephens et al. 2011), but these are unlikely to represent the typical case.

[12] The typical overhead for phase, flux, and bandpass calibration with the EVLA is about 25%.

[13] https://science.nrao.edu/facilities/evla/calibration-and-tools/exposure

have similar radio light curves to those expected for NS–NS mergers (since they produce ejecta with $\beta \sim 0.3$), they are generally less energetic, with only $\sim 10^{47}$–10^{48} erg coupled to the fast ejecta (Berger et al. 2002, 2003). These events will also be accompanied by optical supernova emission on a similar timescale, providing an additional source of discrimination. Finally, relativistic Type Ib/c supernovae (with or without an associated GRB) have $\sim 10^{49}$–10^{50} erg coupled to their fast ejecta (Kulkarni et al. 1998; Soderberg et al. 2010), but these are also accompanied by a bright optical supernovae.

To conclude, the utility of radio emission as an EM counterpart is particularly sensitive to the typical energy and circumburst density. In the case of off-axis afterglows, detections require a high energy and density that exceed those of known SGRB afterglows (Figure 6). In the non-relativistic case, even higher energy and/or density are required, such that for an expected upper bound of $n \lesssim 1$ cm^{-3} the required energy is $E \gtrsim 10^{51}$ erg. The required telescope time for an effective search is hundreds of hours (EVLA), with perhaps only tens of hours using future wide-field instruments (e.g., ASKAP). The time delays range from months to years, which may complicate a robust association. The key advantages are the spherical geometry at $t \gtrsim t_{\rm dec}$ and the smaller number of contaminating sources compared to the optical band.

4. KILONOVA

The detectability of SGRBs and their afterglows is sensitive to uncertainties in the degree of relativistic beaming and, in the case of afterglows, the properties of the circumburst environment. Of course, it is also possible that not all NS–NS mergers produce SGRBs. However, independent of this association, the mergers are expected to be accompanied by isotropic thermal emission, powered by the radioactive decay of heavy elements in the merger ejecta (Li & Paczyński 1998, hereafter LP98; Kulkarni 2005; Rosswog 2005; Metzger et al. 2010b; Roberts et al. 2011; Goriely et al. 2011). Unlike Type Ia supernovae, which are powered by the decay of ^{56}Ni and ^{56}Co, the ejecta from NS–NS mergers is primarily neutron-rich (electron fraction $Y_e \ll 0.5$) and thus produces little nickel. Instead, heavier radioactive elements (mass number $A \gtrsim 130$) are expected to form as neutrons capture onto nuclei (r-process nucleosynthesis) after the ejecta decompresses from nuclear densities (e.g., Lattimer & Schramm 1974; Eichler et al. 1989; Freiburghaus et al. 1999; Metzger et al. 2010a). Although the r-process itself lasts at most a few seconds, these newly synthesized elements undergo nuclear fission and beta decays on much longer timescales. The resulting energy release will power bright emission once the ejecta expands sufficiently that photons can escape.

Neutron-rich material is expected to be ejected both dynamically during the final coalescence (e.g., Rosswog et al. 1999) and by outflows from the accretion disk at later times (e.g., Metzger et al. 2008a, 2009; Dessart et al. 2009; Lee et al. 2009; Figure 1). Depending on the properties of the merging binary, expected values for the ejecta mass and velocity are in the range $M_{\rm ej} \sim 10^{-3}$ to $0.1\,M_\odot$ and $\beta \approx 0.1$–0.3, respectively (e.g., Rosswog et al. 1999; Rosswog 2005). The resulting emission peaks when photons are able to diffuse through the ejecta on the expansion timescale (Arnett 1982); the low ejected mass thus results in a somewhat dimmer and faster evolving light curve than a normal supernova, lasting days instead of weeks.

Metzger et al. (2010b) use a nuclear physics reaction network to calculate the radioactive heating of the ejecta from NS mergers, and a radiative transfer code to model the light curve and color evolution. For typical values of $M_{\rm ej} = 10^{-2}\,M_\odot$ and $\beta = 0.1$, they find that the transient peaks at an absolute visual magnitude of $M_V \simeq -15$ on a timescale of $\sim$1 day; because this is approximately one thousand times brighter than novae (yet dimmer than *super*-novae) they dub these events kilonovae.[14]

Although the calculations of Metzger et al. (2010b) include full radiative transfer, they show that the kilonova light curve is well-approximated using a simple one-zone model (LP98), provided that one adopts a value of $f_{\rm nuc} \approx 3 \times 10^{-6}$ for the dimensionless parameter quantifying the amount of nuclear heating on a timescale of $\sim$1 day (LP98). Similar results for the radioactive heating were found recently by Roberts et al. (2011) and Goriely et al. (2011), despite somewhat different assumptions about the geometric structure and thermodynamics of the ejecta.

In Figures 3 and 4 we plot a range of kilonova models that span the expected range of ejecta mass and velocity, allowing also for realistic theoretical uncertainties in the value of $f_{\rm nuc}$ and the opacity of pure r-process ejecta. The resulting kilonova emission peaks on a timescale of $\sim$0.5–5 days, with an optical luminosity in the range $\sim 10^{41}$–$10^{42.5}$ erg s^{-1}, corresponding to $\approx$19–22.5 mag at the edge of the ALIGO/Virgo volume. Following the peak, the kilonova luminosity declines as $L_\nu \propto t^{-\alpha}$, with $\alpha \approx 1$–1.4, due to the declining radioactive power; the actual light curve may decline even faster once γ-rays or β-decay leptons freely escape the ejecta without depositing their energy.

An important characteristic of kilonovae are their relatively unique spectra, which can serve to distinguish these events from other astrophysical transients. Overall, the kilonova spectrum is predicted to be quasi-thermal with $T \approx 10^4$ K (although line blanketing in the UV may substantially redden the color temperature). Near peak, Doppler broadening caused by the high ejecta velocity will smear out individual spectral features and the overall continuum will be smooth. Following the peak, however, the photosphere will recede deeper into the ejecta, where the velocity is lower. Individual spectral lines from resonant transitions may then become apparent. Since the ejecta are composed entirely of exotic heavy nuclei, the dominant spectral features may not resemble those of any supernova detected to date. Detailed predictions of kilonova spectra are unfortunately impossible because laboratory data on the spectral lines of r-process elements are currently sparse (e.g., Lawler et al. 2009); the closest known analog to a pure r-process photosphere are ultra metal-poor stars in the Galactic halo (e.g., Sneden et al. 2003).

If short GRBs are indeed associated with NS mergers, then kilonovae could in principle be detected with prompt follow-up observations. Unfortunately, for on-axis events the non-thermal afterglow is typically brighter than the predicted kilonova emission (Figure 3). Perhaps the most promising candidate kilonova detection to date was following GRB 080503, which showed an unusual rise in its optical afterglow light curve at $t \sim 1$ day, before rapidly fading over the next several days (Perley et al. 2009). The observed light curve evolution of this event was largely consistent with that expected from a kilonova. However, although the event was well localized on the sky, no obvious host galaxy was detected coincident with the burst, despite the

[14] The terms *mini-supernovae* (LP98) and *macro-novae* (Kulkarni 2005) are also sometimes applied.

Table 1
Comparison of Electromagnetic Counterparts

Counterpart	Detection Efficiency Fraction	Depends on Density?	Virtues Satisfied	Follow-up Instruments
Short GRB (Section 2)	$\sim 3.4 \times f_{b,\gamma} \times \mathrm{FOV}_\gamma$ [a]	no	1,3	*Fermi*/GBM
Orphan optical afterglow (Section 3.1)	$\sim 7\bar{\theta}_j^2 \times \mathcal{F}_{\rm opt}(E_j, n)$ [b] $\lesssim 0.1$	yes	1,3(?),4	Pan-STARRS, LSST
Orphan radio afterglow (Section 3.2)	$\sim 1 \times \mathcal{F}_{\rm rad}(E_j, n)$ [c]	yes	1,3,4(?)	EVLA, ASKAP
Non-relativistic radio (Section 3.2)	?; only if $E \gtrsim 10^{51}$ erg	yes	1(?),3(?),4(?)	EVLA, ASKAP
Kilonova (Section 4)	~ 1 [d]	no	1,2,3(?),4	PTF, Pan-STARRS, LSST

Notes.
[a] Field of view of gamma-ray telescope as a fraction of 4π steradian.
[b] Fraction of mergers accompanied by a sufficiently energetic jet and dense circumburst medium for an optical detection (related to $\mathrm{FOM}_{\rm opt,off} \equiv E_{j,50}\, n_0^{7/8} \gtrsim 0.002$; Equation (2)).
[c] Fraction of mergers accompanied by a sufficiently energetic jet and dense circumburst medium for a radio detection (related to $\mathrm{FOM}_{\rm rad} \equiv E_{j,50}\, n_0^{7/8} \gtrsim 0.2$; Equation (7)).
[d] Assuming that a telescope similar to LSST covers the GW sky error region with a cadence of $\sim$1 day.

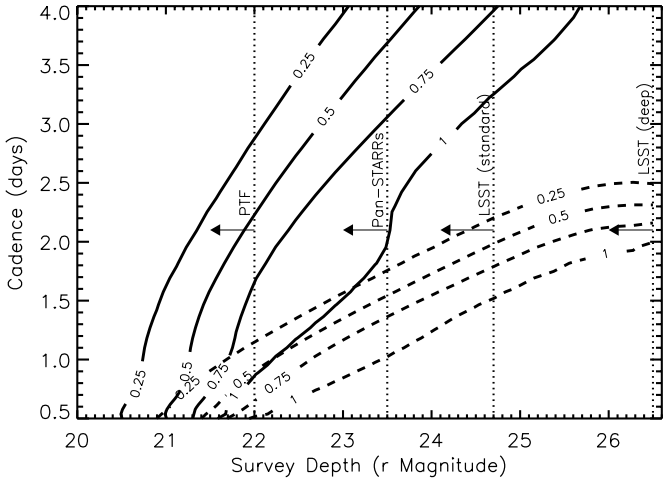

Figure 8. Fraction of kilonova events detected in three (solid line) or five (dashed line) epochs as a function of the depth and cadence of a search. We have adopted a representative kilonova model with $M_{\rm ej} = 10^{-2}\, M_\odot$, $\beta = 0.1\, c$, and $f_{\rm nuc} = 3 \times 10^{-6}$.

relatively low redshift required to explain the observed peak brightness.

To assess the detectability of kilonovae we carry out a Monte Carlo simulation for optical surveys with a range of limiting magnitudes and cadences (Table 3). We find that at the depth and cadence of the normal LSST survey ($r \approx 24.7$ mag, $\Delta t = 4$ days), essentially no kilonovae will be detected in five epochs, unless $M_{\rm ej} \sim 0.1\, M_\odot$; about three-fourths of all events will be detected in three epochs with the normal LSST survey if $M_{\rm ej} \sim 10^{-2}\, M_\odot$. To detect events with $M_{\rm ej} \sim 10^{-2}\, M_\odot$ in five epochs requires a one-day cadence, preferably with telescopes capable of reaching $\gtrsim$23 mag (e.g., Pan-STARRS, LSST). Finally, for $M_{\rm ej} \sim 10^{-3}\, M_\odot$, no existing or planned telescope will provide five detections, but LSST with a one-day cadence is likely to provide three to four detections. These results are also summarized in Figure 8, where we plot contours for the fraction of kilonovae detected in three and five epochs as a function of limiting magnitude and cadence, assuming typical values of $M_{\rm ej} = 10^{-2}\, M_\odot$, $\beta = 0.1$, and $f_{\rm nuc} = 3 \times 10^{-6}$. The plot demonstrates that to achieve 50% completeness in 3(5) epochs given a cadence of $\sim$1 day requires a limiting magnitude of $\gtrsim$21(22.5) mag. We discuss potential contamination from other optical transients in Section 5.

5. SUMMARY: WHAT IS THE MOST PROMISING EM COUNTERPART?

We now bring together our conclusions from the previous sections to address the question of the most promising EM counterpart. A summary of the expected detection fractions, dependence on density, and the Cardinal Virtues satisfied for each EM counterpart is provided in Table 1. We first discuss the case in which all NS–NS mergers are accompanied by SGRBs, and hence by on-axis γ-ray/afterglow emission or by off-axis afterglow emission; we then turn to a discussion of the kilonova-dominated case.

5.1. Gamma-Rays

Short GRBs are easily detectable within the ALIGO/Virgo volume with current γ-ray satellites in cases when $\theta_{\rm obs} \lesssim \theta_j$; they therefore satisfy Virtue 1. Although this configuration applies to only a small fraction of all mergers (and therefore violates Virtue 2), the SGRB rate within the ALIGO/Virgo volume (enhanced by a factor of 3.4 for face-on mergers) is sufficiently high that $\sim$1 coincident event should occur per year (Figure 2). SGRBs thus represent an ideal counterpart to confirm the cosmic origin of at least some GW events and to test whether SGRBs in fact accompany NS–NS/NS–BH mergers. Such an association is critical since it will help to justify the expensive search for orphan afterglows in the optical and radio bands. SGRBs also suffer from little contamination and therefore satisfy Virtue 3. It is therefore critical that a sensitive γ-ray satellite be in operation during the ALIGO/Virgo era. Fine positional accuracy for an SGRB detection (e.g., *Swift*) is less critical than all-sky coverage (e.g., *Fermi*/GBM) since the temporal association alone within the large error region of a GW source would suffice to determine an association. A $\sim$arcsecond position (satisfying Virtue 4) could then be achieved from the expected on-axis optical afterglow or a kilonova, which will be brighter than $\sim$22 mag and hence easily detectable with wide-field telescopes. Thus, SGRBs satisfy three out of the four virtues for a promising EM counterpart.

5.2. Off-axis Optical and Radio Afterglows

In the absence of γ-ray emission, orphan afterglow emission (both optical and radio) is the most promising counterpart if the typical jet energy and circumburst density lie near the upper end estimated from current SGRB observations: $E_{j,50}^{4/3}\, n_0^{1/2} \sim 0.1$.

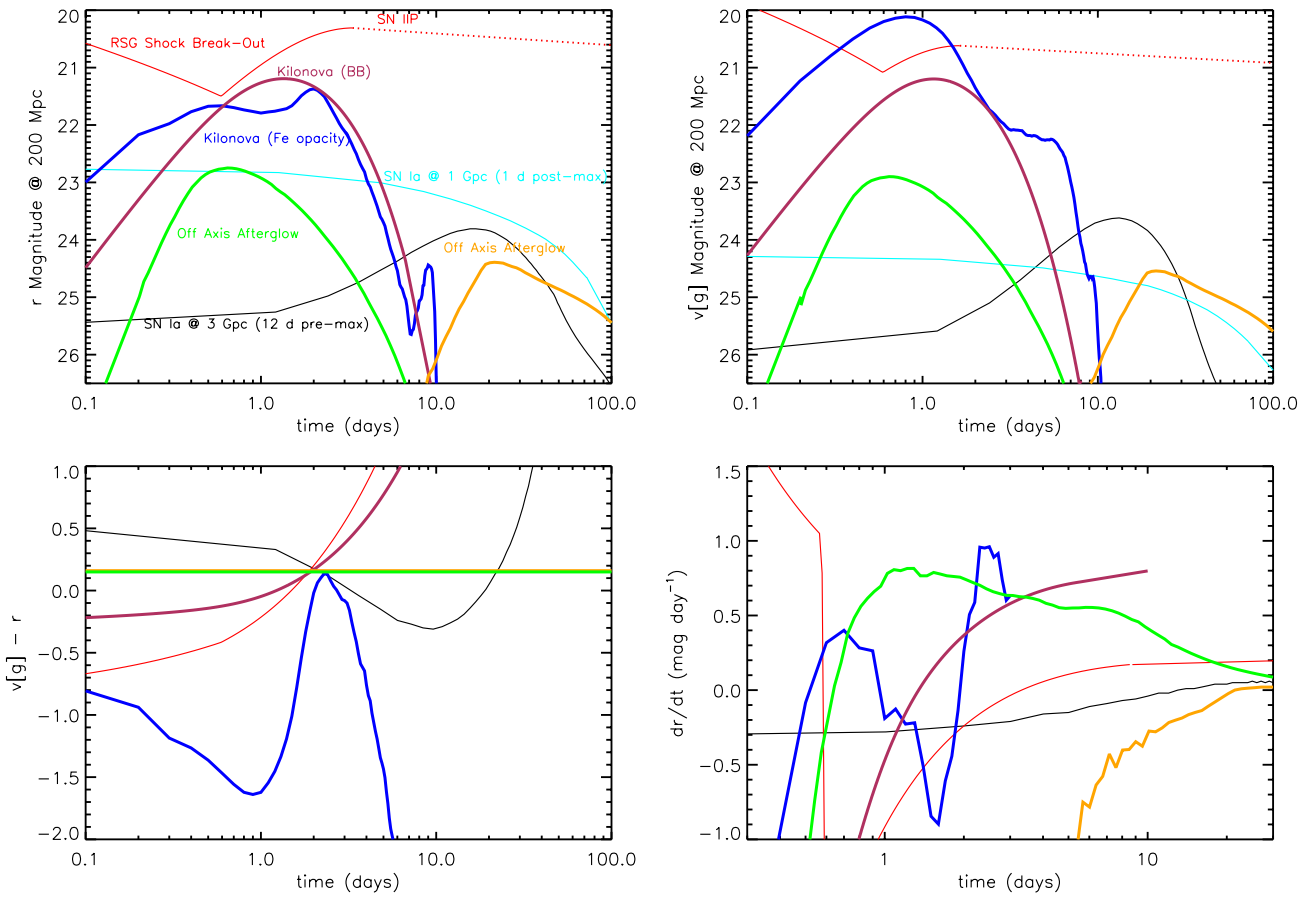

Figure 9. Comparison of off-axis afterglow and kilonova light curves with contaminating optical transients, including r-band light curve (top left), V-band light curve (top right), $V - r$ color curves (bottom left), and r-band decline rate (bottom right). Off-axis light curves are shown for the parameters in Figures 3–5. We use a typical model for the kilonova light curve, $M_{\rm ej} = 10^{-2}\,M_\odot$ and $\beta = 0.1$, for two different assumptions about the opacity of the ejecta: the LP98 model assuming blackbody emission (purple), and a model assuming pure Fe opacity from Metzger et al. (2010b) (blue). Shown for comparison are background Type Ia supernova light curves 12 days before maximum (black) and 1 day after maximum (cyan) from Wang et al. (2009), as well as supernova shock breakout from a red supergiant (red) (Nakar & Sari 2010), followed by a standard Type IIP supernova plateau (dashed red).

(A color version of this figure is available in the online journal.)

For off-axis optical afterglows the detectability limit with LSST is $\mathrm{FOM}_{\rm opt,off} \equiv E_{j,50}\,n_0^{7/8} \gtrsim 0.002$, as long as $\theta_{\rm obs} \lesssim 2\theta_j$. Thus, optical afterglows satisfy Virtue 1, but violate Virtue 2 since a fraction of at most $\sim 7\bar{\theta}_{\rm j}^2 \sim 0.1$ would be detectable. For radio afterglows the detectability limit with EVLA or a future instrument like ASKAP is $\mathrm{FOM}_{\rm rad} \equiv E_{j,50}\,n_0^{7/8} \gtrsim 0.2$ independent of viewing angle (i.e., they satisfy Virtue 2). However, as a result of the limited range of E–n phase space probed by radio observations, they violate Virtue 1. Indeed, using the tracks for existing SGRB optical afterglows in the E–n phase space, we find that none cross the portion accessible to radio searches (Figure 6). It is therefore possible that despite the relative isotropy of the radio emission, existing and planned instruments are simply not sensitive enough to detect the emission for typical SGRB parameters. On the other hand, about half of all existing optical afterglows will be detectable to the depth of LSST (Figure 6), but only with a viewing angle up to $\sim 2\theta_j$, indicating an expected optical detection fraction of $\lesssim 5\%$.

In terms of Virtue 3, contamination in the radio band is less severe than in the optical band. In the optical, we expect contamination mainly from background supernovae (Type Ia, and Type IIP shock breakout), while contamination from AGN variability can be avoided based on its coincidence with a galaxy nucleus. We evaluate the off-axis light curves in comparison to supernova light curves in Figure 9. For the high-density case ($n \sim 1$ cm^{-3}), the off-axis light curve peaks on a timescale of $\sim$1 day, and is indeed similar to the kilonova light curves. The rapid rise and decline (declining by $\sim$3 mag in $\sim$5 days) can easily distinguish this case from Type Ia supernovae, which rise and decline by comparable amounts on timescales of tens of days (Figure 9). Shock breakout emission from red supergiants also leads to rapid rise and decline ($\sim$1 mag on a timescale of $\sim$1 day), but is subsequently followed by a long and bright plateau phase (a Type IIP supernova) that can easily distinguish these cases. Thus, with a sufficiently rapid cadence (one day) and a depth similar to the LSST normal survey (or better yet $\sim$0.5 hr pointings with $\approx$26.5 mag), off-axis afterglows in a dense medium can be separated from background contaminating supernovae.

The case of an off-axis afterglow in a low-density medium ($n \sim 10^{-3}$ cm^{-3}) is somewhat more complicated. The off-axis light curve peaks on a timescale of $\sim$20 days, followed by a decline of about 1 mag in the subsequent three months (Figure 9). With a peak brightness of $\sim$24.5 mag, a convincing detection requires a depth beyond the normal LSST survey mode. However, a one-day cadence is not essential, and the depth can be achieved by stacking multiple images on a $\sim$one-week timescale. Given the slower evolution of the light curve, it is more similar to supernova light curves than the $n \sim 1$ cm^{-3}

case. The predicted rate of decline is slower than a Type Ia supernova post maximum (i.e., ≈2.5–3 mag in ∼100 days). It is, however, faster than a typical Type IIP supernova light curve, which exhibits a plateau for ∼100 days.

Color evolution can in principle also be used to distinguish off-axis afterglows from other transients. Since the afterglow is synchrotron emission (and the optical waveband is generally above the characteristic frequency, ν_m), it has a power-law spectrum with a fixed slope $F_\nu \propto \nu^{(1-p)/2}$ and hence a constant red color $g-r \sim 0.2$ mag for $p = 2.5$. By comparison, Figure 9 shows that the color of a shock breakout and rising Type IIP supernovae increases by a magnitude from blue to red in just a few days. Although the colors of a rising Type Ia supernova are similar to the afterglow emission, events observed near their peak (the case in which a background Type Ia supernova light curve could be mistaken for a low-density afterglow) are much redder.

Finally, both radio and optical counterparts will satisfy Virtue 4, although at low frequency and low S/N, EVLA/ASKAP positions will typically be $\gtrsim$few arcsec, as opposed to subarcsecond in the optical band. At a typical distance of 200 Mpc this should not be an impediment for a host galaxy association ($1'' \approx 0.8$ kpc), but it will not allow a robust study of the sub-galactic environment, and hence an association with specific stellar populations (cf. Fong et al. 2010). It may also impede the rejection of AGNs.

We therefore conclude that optical and radio afterglows do not satisfy all of the required Cardinal Virtues for an EM counterpart. The fraction of detectable off-axis optical afterglows is ∼0.1, and possibly even lower depending on the range of energy and circumburst density for typical NS–NS/NS–BH mergers. The fraction of detectable radio afterglows may be close to zero due to the limited range of E–n phase space accessible with existing and planned radio telescopes.

5.3. Kilonova

If the majority of NS–NS/NS–BH mergers occur in low-density environments ($n \lesssim 10^{-3}$ cm^{-3}) or produce low-energy jets ($E \lesssim 10^{49}$ erg), then optical afterglows are no longer effective counterparts. This is also true if most NS–NS mergers are not accompanied by SGRBs. In these cases, kilonovae provide an isotropic source of emission that does not depend on the external environment. Because the emission is thermal and requires only a small quantity of neutron-rich ejecta (as is likely to accompany most mergers), the predicted signal is also relatively robust, and at a peak optical brightness of ∼19–22 mag is detectable with a facility such as LSST. Thus, kilonovae satisfy Virtues 1, 2, and 4, as long as a rapid and deep search is carried out (Figure 8 and Table 3). Therefore, a key question is whether these events can be easily distinguished from contaminating sources (cf. Kulkarni & Kasliwal 2009).

We present kilonova light curves in comparison to background supernovae in Figure 9. We show both a blackbody model (LP98) and a model assuming pure Fe opacity (Metzger et al. 2010b) to span the plausible range in the true light curve and color evolution, the latter of which remains especially uncertain due to the lack of experimental data on the opacity of pure r-process ejecta. As in the case of off-axis afterglow emission in a dense medium, the kilonova light curve evolution is much more rapid than for supernovae: the rise time is ∼1 day, followed by a decline of about 3 mag in ∼5–8 days. This behavior places stringent constraints on an effective search (one-day cadence and a depth of $\gtrsim$24 mag), but it allows for a clean separation from contaminating supernovae. Thus, it appears that kilonovae can satisfy all four Cardinal Virtues.

5.4. Quality of Information: A Fifth Virtue?

Even if all types of EM counterparts discussed in this paper will eventually be detected in conjunction with GW triggers, each provides distinct information about the merger. The detection of an SGRB in temporal coincidence with a GW trigger will establish a firm connection with NS–NS/NS–BH mergers. Since these events are also expected to be face-on mergers, such a detection will establish the orientation of the binary, thereby allowing for more accurate extraction of additional binary parameters from the GW signal, such as the masses and spins of its members and, potentially, information about the high-density equation of state. While a γ-ray detection itself will not provide a position with arcsecond accuracy, an on-axis optical afterglow, or a kilonova, should be detectable and will provide a host galaxy association and redshift.

The detection of an orphan optical afterglow (on- or off-axis) will provide much of the same information. Namely, it will establish a connection with SGRBs and will also possess a nearly face-on orientation (since orphan optical afterglows are only detectable to $\lesssim 2\theta_j$). The brightness of the optical emission will also provide information on the combination of energy and circumburst density. A radio detection will provide no information on binary orientation (since essentially all off-axis angles are detectable). The peak time and brightness will provide information on the combination of energy, density, and ejecta velocity. As a result of the velocity degeneracy, a radio detection will not necessarily establish an association with SGRBs (i.e., the specific case of $\beta \approx 1$). Finally, kilonova detections provide a unique probe of the inner workings of the merger, since their light curves depend on the mass, velocity, and geometry of the ejecta, while their opacity and spectral features probe the ejecta composition (spectroscopy will require real-time identification near peak). The discovery of a kilonova event will also represent the first in situ observation of freshly produced r-process material, the origin of which remains perhaps the biggest mystery in nuclear astrophysics. However, such detections will not help to establish a connection with SGRBs.

To summarize, the potential connection of NS–NS mergers with SGRBs provides a useful EM counterpart for both on- and off-axis emission. However, in essentially all possible scenarios, only a small fraction of GW events ($\lesssim$10%) will be followed by a detectable SGRB or optical/radio afterglow. On the other hand, isotropic kilonovae will likely provide a larger detection fraction, as long as the typical ejected mass is $\gtrsim 10^{-3}\,M_\odot$ and deep observation with one-day cadence are carried out.

6. FOLLOW-UP STRATEGY RECOMMENDATIONS

Taking advantage of any of the potential EM counterparts discussed in the previous sections requires a careful observing strategy. In this section we make specific recommendations for searches at γ-ray, optical, and radio wavelengths to enhance the detection probability, *given a reasonable allocation of resources*.

6.1. Gamma-Rays

In the case of γ-ray detections of an associated SGRB, the limiting factor is the small fraction of on-axis events within the ALIGO/Virgo detection volume. The on-axis orientation

provides a boost to the detection volume, leading to a detectable rate perhaps as high as ∼1 event per year. As a result of this low rate, all-sky coverage in γ-rays is more critical than the ability to substantially refine the GW positions. This will still allow for a robust association due to the temporal coincidence, and the positional refinement can then be achieved from the bright on-axis optical afterglow. In addition, since a temporal coincidence with an SGRB allows for a lower threshold GW detection, a strategy of searching the GW data stream based on γ-ray triggers may actually lead to a larger number of detections than the opposite approach (i.e., it will boost the accessible volume by more than a factor of 3.4 times for face-on orientation). Thus, we strongly recommend an operational γ-ray satellite in the ALIGO/Virgo era, with capabilities similar to the *Fermi*/GBM. The major advantage of *Fermi*/GBM is its wide FOV compared to the *Swift* Burst Alert Telescope, although *Swift* would provide a better localization (a few arcminutes versus degrees) for those rare events in its field.

6.2. Optical

The search for orphan optical afterglows requires wide-field telescopes capable of achieving a depth of at least ∼23 mag, and perhaps ∼26.5 mag for detections of typical events. The maximum achievable depth is determined by the need to cover tens of square degrees with a one-day cadence. Since ∼10 pointings are required with facilities such as PTF, Pan-STARRS, and LSST, the maximum time per pointing is about 0.5 hr, leading to depths of ∼22 mag for PTF, ∼23.5 mag for Pan-STARRS, and ∼26.5 mag for LSST. For a localization region of a few square degrees (i.e., a single pointing), the achievable limiting magnitudes are about 1.2 mag deeper. The results of Monte Carlo simulations of the detection fractions in three and five epochs for on- and off-axis afterglows given a limiting magnitude and cadence are summarized in Table 2 and Figure 7. We find that only in the case of $E \sim 10^{50}$ erg are the standard LSST cadence and depth sufficient for multiple detections. However, for lower energies (which may be typical of most SGRBs), a faster cadence and greater depth (∼26.5 mag) are required for multiple detections. To achieve a detection fraction of 50% in 3(5) epochs for the case of $E_j \sim 10^{48}$ erg and $\theta_{\rm obs} = 2\theta_j$ requires a depth of at least 23.5(26) mag for a one-day cadence. Thus, we conclude that standard LSST depth and cadence are non-ideal for detections of off-axis afterglows.

A key issue discussed in previous papers is that at the typical distance limit of ∼200 Mpc for ALIGO/Virgo detections, one could expedite the search for EM counterparts by focusing on galaxies within this volume. However, the number of galaxies within a typical GW error region in the typical luminosity range of SGRB hosts ($L \gtrsim 0.1\,L^*$) is[15] ∼400; the number of L^* galaxies is about 50. Thus, the number of galaxies is much larger than the required number of pointings for wide-field telescopes (∼10), and therefore a focus on nearby galaxies has no effect on the required cadence and depth. Conversely, the number of galaxies is too large for an efficient search with a large-aperture but small-FOV telescope (e.g., Keck, Gemini) since several hundred pointings will be required within a single night (leading to $\lesssim$1 minute per pointing). Even a search of only $L \gtrsim L^*$ galaxies (which will inevitably miss a substantial fraction of the counterparts in sub-L^* galaxies) will limit the observations to ∼5 minutes per galaxy, and will require the full use of an 8 m class telescope for several nights.

Thus, our key recommendation is follow-up with wide-field optical telescopes capable of reaching a depth of $\gtrsim$23 mag in 0.5 hr, using a one-day cadence. Effectively, this means that LSST should execute a non-standard cadence to follow up GW triggers (a "sub-survey" mode). Ideally, such dedicated follow-up observations will also involve longer exposure times than the normal survey mode (up to ∼0.5 hr per pointing), but even without a change to the standard exposure time, repeated visits on a nightly basis will provide the most efficient search strategy for optical counterpart searches. The same strategy is key for detections of the fast-evolving kilonovae (Figure 8 and Table 3). If no convincing counterpart is detected within a few days, a search for delayed off-axis emission (due to low density) can employ the normal LSST cadence since the typical timescale is tens of days (Figure 7).

We note that efforts to perform GW-triggered optical follow-up have already begun during the recent LIGO science run by the LOOC UP (Locating and Observing Optical Counterparts to Unmodeled Pulses) project (Kanner et al. 2008; Abbott et al. 2008; The LIGO Scientific Collaboration & Virgo Collaboration 2011). LOOC UP reconstructs the sky position of candidate GW signals to make prompt optical follow-up observations using

Table 2
Detection Efficiency of Orphan Afterglows within 200 Mpc

$r_{\rm lim}$ (AB mag)	Δt (days)	$E_{\rm j}$ (erg)	n (cm^{-3})	$\theta_{\rm obs}$	$f_{\rm det,1}$	$f_{\rm det,3}$	$f_{\rm det,5}$
22.0	1	10^{48}	1	θ_j	1.00	0.05	0.00
23.5	1	···	···	···	1.00	0.40	0.02
24.7	4	···	···	···	1.00	0.00	0.00
24.7	1	···	···	···	1.00	0.95	0.08
26.5	1	···	···	···	1.00	0.95	0.80
22.0	1	···	···	$2\theta_j$	0.28	0.05	0.00
23.5	1	···	···	···	1.00	0.37	0.07
24.7	4	···	···	···	0.95	0.01	0.00
24.7	1	···	···	···	1.00	1.00	0.37
26.5	1	···	···	···	1.00	1.00	1.00
26.5	1	···	···	$4\theta_j$	0.18	0.18	0.18
22.0	1	···	10^{-3}	θ_j	0.34	0.00	0.00
23.5	1	···	···	···	0.56	0.01	0.00
24.7	4	···	···	···	0.38	0.00	0.00
24.7	1	···	···	···	1.00	0.10	0.02
26.5	1	···	···	···	1.00	0.93	0.29
26.5	1	···	···	$2\theta_j$	0.00	0.00	0.00
22.0	1	10^{50}	1	θ_j	1.00	1.00	1.00
24.7	4	···	···	···	1.00	1.00	1.00
22.0	1	···	···	$2\theta_j$	1.00	1.00	1.00
24.7	4	···	···	···	1.00	1.00	1.00
22.0	1	···	···	$4\theta_j$	0.05	0.05	0.05
23.5	1	···	···	···	0.39	0.39	0.39
24.7	4	···	···	···	1.00	1.00	1.00
26.5	1	···	···	···	1.00	1.00	1.00
22.0	1	···	10^{-3}	θ_j	1.00	1.00	1.00
24.7	4	···	···	···	1.00	1.00	1.00
23.5	1	···	···	$2\theta_j$	0.27	0.27	0.27
24.7	4	···	···	···	1.00	1.00	1.00
26.5	1	···	···	$4\theta_j$	0.03	0.03	0.03

Notes. The columns are (left to right): (1) 5σ r-band limiting magnitude; (2) observing cadence; (3) jet energy; (4) density; (5) viewing angle; (6) fraction of events detected in one epoch; (7) fraction of events detected in three epochs; and (8) fraction of events detected in five epochs.

[15] We use the SDSS luminosity function with $M_r^* \approx -21.2$ mag and $\phi^* \approx 5 \times 10^{-3}$ Mpc^{-3} (Blanton et al. 2003). Integration down to $0.1\,L^*$ therefore gives about eight galaxies per square degree within a distance of 200 Mpc.

Table 3
Detection Efficiency of Kilonovae within 200 Mpc

$r_{\rm lim}$ (AB mag)	Δt (days)	$M_{\rm ej}$ ($M_\odot$)	$v_{\rm ej}$ (c)	$f_{\rm nuc}$	$f_{\rm det,1}$	$f_{\rm det,3}$	$f_{\rm det,5}$
22.0	1	10^{-1}	0.1	3×10^{-6}	1.00	1.00	1.00
24.7	4	...	...	...	1.00	1.00	1.00
22.0	1	10^{-2}	...	...	1.00	0.89	0.37
23.5	1	...	...	...	1.00	1.00	0.96
24.7	4	...	...	...	1.00	0.73	0.00
24.7	1	...	...	...	1.00	1.00	1.00
23.5	1	...	...	1.5×10^{-6}	1.00	0.89	0.22
23.5	1	...	...	6×10^{-6}	1.00	1.00	1.00
22.0	1	...	0.3	3×10^{-6}	1.00	0.89	0.03
23.5	1	...	...	...	1.00	0.98	0.20
24.7	4	...	...	...	0.93	0.05	0.05
24.7	1	...	...	...	1.00	1.00	0.73
26.5	1	...	...	...	1.00	1.00	1.00
22.0	1	10^{-3}	0.1	...	0.24	0.06	0.00
23.5	1	...	...	...	1.00	0.47	0.00
24.7	4	...	...	...	0.56	0.00	0.00
24.7	1	...	...	...	1.00	0.94	0.00
26.5	1	...	...	...	1.00	0.98	0.00

Notes. The columns are (left to right): (1) 5σ r-band limiting magnitude; (2) observing cadence; (3) ejecta mass; (4) ejecta velocity; (5) nuclear heating parameter (Li & Paczyński 1998); (6) fraction of events detected in one epoch; (7) fraction of events detected in three epochs; and (8) fraction of events detected in five epochs.

wide-field sub-meter-class telescopes. Cannon et al. (2011) discuss techniques to reduce the latency between GW detection and follow-up to minutes or even seconds, in which case counterpart searches could in principle begin simultaneous with the final coalescence. The meter-class telescopes employed in LOOC UP were sufficiently sensitive to detect off-axis afterglows or kilonova within the LIGO volume, but will be clearly insufficient for the ALIGO/Virgo volume.

6.3. Radio

The search for radio counterparts is complicated by the highly uncertain peak time of the light curve (ranging from months to years), as well as by the small FOV of the EVLA. For an off-axis afterglow in a dense medium the expected peak time is ∼0.1 yr, while for a non-relativistic spherical counterpart the expected peak occurs on a timescale of a few years. As a result, a robust search has to cover a broad range of timescales, with an initial rapid cadence of ∼1 week, followed by a transition to monthly and then yearly observations. In total we estimate that at least 10–15 epochs will be required, spread logarithmically over a decade. As discussed in Section 3.2, a search with the EVLA will require about 30 hr per epoch to cover a typical GW error region. If we assume that about half of these epochs will take place within the first year after the trigger, the required time to follow up the best-bet rate of 40 GW triggers per year is about 100% of the EVLA time.

The peak flux density required for a convincing detection (a factor-of-two rise above the achievable $5\sigma = 0.25$ mJy threshold) is about 0.5 mJy. As shown in Figure 6, none of the existing SGRB optical afterglows will lead to such a bright signal. The detection of events with $F_{\nu,p} \sim 0.1$ mJy is complicated not only by the excessive amount of required telescope time (hundreds of hours per epoch!), but also by source confusion at low frequency, and the fact that a host galaxy with SFR $\sim 1\ M_\odot\ {\rm yr}^{-1}$ has a 1 GHz flux density of ∼0.6 mJy. These factors will limit the searches even if the error regions are only a few square degrees.

In terms of the search strategy, at 1 GHz the best approach is to tile the full error region with ∼100–200 pointings, while at higher frequencies it is more profitable to target the ∼400 galaxies with $L \gtrsim 0.1\ L^*$ individually (although this will require even more observing time). Observations with a future facility such as ASKAP will reduce the time requirement to a few hours per epoch by reducing the number of pointings. However, the sensitivity of the search is unlikely to improve since source confusion becomes a dominant obstacle.

We finally note that for the case of radio emission from non-relativistic ejecta, the required energy and density are $E \gtrsim 10^{51}$ erg and $n \gtrsim 0.1\ {\rm cm}^{-3}$ (Figure 6), respectively. It is unclear if the required energy scale can be produced in a typical NS–NS merger, but even if it does, the resulting decade-long delay between the GW trigger and peak of the putative radio emission will require many observing epochs, and will furthermore impede a convincing association.

Thus, our recommendation in the case of radio searches is to limit the search to a timescale of a few months, appropriate for the case of an off-axis afterglow ($\beta \sim 1$). In this case the peak brightness is also more likely to be detectable, since $F_{\nu,p} \propto \beta^{11/4}$, and the relatively modest time delay ($t_{\rm dec} \propto \beta^{-5/3}$) will reduce the potential for contamination. The required observing time with the EVLA will be about ∼200 hr for several epochs logarithmically spaced in time over several months. Future searches with facilities like ASKAP should also focus on the same timescale since they are limited to the same depth as EVLA.

7. CONCLUSIONS

With the era of GW astronomy fast approaching we investigated and critically assessed a range of potential EM counterparts for NS–NS/NS–BH mergers, and their detectability with existing and upcoming telescopes. We used the rates of (on-axis) SGRBs to predict the detection rate with an all-sky γ-ray monitor, and existing information about SGRB afterglows to predict the appearance and brightness of off-axis optical and radio emission. Finally, we assessed the light curves and detectability of kilonovae. Overall, we found that none of the potential EM counterparts is guaranteed to satisfy all four Cardinal Virtues—detectability, high fraction, identifiability, and positional accuracy—but that critical insight into the merger physics can be gained from any of the counterparts for at least some events. In particular, we found that:

1. Gamma-ray and/or hard X-ray observations are critical for establishing a firm connection between SGRBs and NS–NS/NS–BH mergers. Such detections are likely to be limited to a rate of $\lesssim 1\ {\rm yr}^{-1}$, but the face-on configuration will allow for better measurements of the binary parameters. In addition, γ-ray-*triggered* GW searches may enhance the probability of joint GW/EM detections.
2. The number of expected galaxies with $L \gtrsim 0.1\ L^*$ (typical of SGRB hosts; Berger 2009) in a typical GW error region is ∼400, making targeted searches of galaxies in the optical and/or radio inefficient. In both cases, complete coverage of the error region is less time consuming.
3. On-axis optical emission typical of existing SGRB afterglows is easily detectable with existing and planned wide-field telescopes at $\lesssim$200 Mpc.

4. Off-axis optical afterglow emission is only detectable to $\theta_{\rm obs} \sim 2\theta_j$ and is hence limited to $\lesssim$10% of all mergers. Within this range, LSST observations are required to detect events similar to existing SGRB afterglows, but with a specialized depth/cadence of $\sim$26.5 mag (achievable in 0.5 hr) and one-day. Observations with the normal LSST survey mode are likely to miss most counterparts. With our proposed LSST depth/cadence, contamination from other sources can be avoided based on the rapid rise and decline time for high-density cases, and based on the decline rate and lack of color evolution for low-density cases.
5. Off-axis radio afterglow emission can in principle be detected at all observer angles, but existing and planned telescopes are limited to flux levels that exclude the detection of existing SGRB afterglows. The long delay relative to the GW trigger (up to many years) provides an additional obstacle to robust association. Still, searches with a weekly–monthly cadence and per-epoch exposure times of $\sim$30 hr (EVLA), or $\sim$few hr (ASKAP), may lead to detections of rare energetic events in a dense medium. Contamination from other sources is less severe than in the optical band, but the positional accuracy of a detection will be poorer than in the optical, potentially preventing studies of sub-galactic environments.
6. Isotropic optical emission powered by the radioactive decay of *r*-process elements in the merger ejecta (kilonova) is expected to reach a peak brightness of $\sim$19–22 mag at $\Delta t \sim$ 1 day, with a subsequent decline by several magnitudes in a few days. The brightness is independent of the ambient density. The detection of kilonovae therefore requires rapid cadence ($\sim$1 day) to at least the normal LSST survey depth (and preferably a maximal depth of $\sim$26.5 mag). The rapid rise and decline will reduce the contamination from other optical transients (e.g., supernovae). With the wherewithal to carry out such a search with LSST, kilonovae can indeed serve as the most promising counterpart of compact object binary mergers.
7. Our key recommendations for maximizing the detection probability of EM counterparts are: an all-sky γ-ray satellite similar to *Fermi*/GBM; a specialized LSST "sub-survey" mode with a one-day cadence and a depth of $\sim$26.5 mag; and radio follow-up with a weekly cadence to a depth of 0.25 mJy using EVLA/ASKAP, limited to $\lesssim$few months after the trigger.

Since the timescales of the various potential EM counterparts are spread from seconds (γ-rays) to days (optical) to months (radio), a staggered approach will clearly inform a joint observational strategy. For example, the detection of γ-ray emission should trigger an immediate high-cadence search for on-axis afterglow/kilonova emission in both the optical and radio; such a search will still require wide-field imaging. Similarly, the detection of off-axis afterglow or kilonova optical candidate(s) should trigger targeted radio observations (allowing for much deeper observations relative to a complete search of the GW error circle).

We finally note that our framework for evaluating potential EM counterparts can be revised as the actual positional capabilities of ALIGO/Virgo and the merger rate become clear. However, unless the GW sensitivity or rate have been substantially overestimated, we conclude that a concerted follow-up effort will determine whether NS–NS/–BH mergers are associated with SGRBs, and will provide critical insight into the physics of compact objects and the merger process. The fundamental importance of these results justifies the proposed expensive EM observational strategy.

We thank Hendrik van Eerten and Andrew MacFadyen for producing and maintaining their online library of afterglow light curves. We thank Ehud Nakar for providing theoretical light curves of supernova shock breakout. We thank S. Nissanke and R. O'Shaughnessy for helpful discussions and information. B.D.M. is supported by NASA through Einstein Postdoctoral Fellowship grant No. PF9-00065 awarded by the Chandra X-ray Center, which is operated by the Smithsonian Astrophysical Observatory for NASA under contract NAS8-03060. E.B. acknowledges support for this work from the National Science Foundation through grant AST-1107973.

REFERENCES

Abadie, J., Abbott, B. P., Abbott, R., et al. 2010a, Class. Quantum Grav., 27, 173001
Abadie, J., Abbott, B. P., Abbott, R., et al. 2010b, ApJ, 715, 1453
Abbott, B., Abbott, R., Adhikari, R., et al. 2008, Class. Quantum Grav., 25, 114051
Abbott, B. P., Abbott, R., Acernese, F., et al. 2010, ApJ, 715, 1438
Abbott, B. P., Abbott, R., Adhikari, R., et al. 2009, Phys. Rev. D, 80, 102001
Abramovici, A., Althouse, W. E., Drever, R. W. P., et al. 1992, Science, 256, 325
Acernese, F., Alshourbagy, M., Antonucci, F., et al. 2009, Class. Quantum Grav., 26, 085009
Aloy, M. A., Janka, H.-T., & Müller, E. 2005, A&A, 436, 273
Arnett, W. D. 1982, ApJ, 253, 785
Barkov, M. V., & Pozanenko, A. S. 2011, MNRAS, 417, 2161
Berger, E. 2007, ApJ, 670, 1254
Berger, E. 2009, ApJ, 690, 231
Berger, E. 2010, ApJ, 722, 1946
Berger, E. 2011, New Astron. Rev., 55, 1
Berger, E., Kulkarni, S. R., & Chevalier, R. A. 2002, ApJ, 577, L5
Berger, E., Kulkarni, S. R., Frail, D. A., & Soderberg, A. M. 2003, ApJ, 599, 408
Berger, E., Price, P. A., Cenko, S. B., et al. 2005, Nature, 438, 988
Blanton, M. R., Hogg, D. W., Bahcall, N. A., et al. 2003, ApJ, 592, 819
Bloom, J. S., Prochaska, J. X., Pooley, D., et al. 2006, ApJ, 638, 354
Bloom, J. S., Holz, D. E., Hughes, S. A., et al. 2009, arXiv:0902.1527
Bucciantini, N., Metzger, B. D., Thompson, T. A., & Quataert, E. 2012, MNRAS, 419, 1537
Burrows, D. N., Fox, D., Palmer, D., et al. 2011, arXiv e-prints
Burrows, D. N., Grupe, D., Capalbi, M., et al. 2006, ApJ, 653, 468
Cannon, K., Cariou, R., Chapman, A., et al. 2011, arXiv:1107.2665
Caron, B., Derome, L., Flaminio, R., et al. 1999, Astropart. Phys., 10, 369
Chawla, S., Anderson, M., Besselman, M., et al. 2010, Phys. Rev. Lett., 105, 111101
Chernoff, D. F., & Finn, L. S. 1993, ApJ, 411, L5
Coward, D. M., Gendre, B., Sutton, P. J., et al. 2011, MNRAS, 415, L26
Dalal, N., Holz, D. E., Hughes, S. A., & Jain, B. 2006, Phys. Rev. D, 74, 063006
Deffayet, C., & Menou, K. 2007, ApJ, 668, L143
Dessart, L., Ott, C. D., Burrows, A., Rosswog, S., & Livne, E. 2009, ApJ, 690, 1681
Duez, M. D., Foucart, F., Kidder, L. E., Ott, C. D., & Teukolsky, S. A. 2010, Classical Quant. Grav., 27, 114106
Eichler, D., Livio, M., Piran, T., & Schramm, D. N. 1989, Nature, 340, 126
Fairhurst, S. 2009, New J. Phys., 11, 123006
Finn, L. S., Mohanty, S. D., & Romano, J. D. 1999, Phys. Rev. D, 60, 121101
Fong, W., Berger, E., Chornock, R., et al. 2011, ApJ, 730, 26
Fong, W., Berger, E., & Fox, D. B. 2010, ApJ, 708, 9
Fox, D. B., Frail, D. A., Price, P. A., et al. 2005, Nature, 437, 845
Freiburghaus, C., Rosswog, S., & Thielemann, F. 1999, ApJ, 525, L121
Gorenstein, P. 2011, Proc. SPIE, 8147, 56
Goriely, S., Bauswein, A., & Thomas Janka, H. 2011, ApJ, 738, L32
Götz, D., Paul, J., Basa, S., et al. 2009, in AIP Conf. Ser. 1133, Gamma-Ray Burst, ed. C. Meegan, C. Kouveliotou, & N. Gehrels (Melville, NY: AIP), 25
Granot, J., & Sari, R. 2002, ApJ, 568, 820
Grupe, D., Burrows, D. N., Patel, S. K., et al. 2006, ApJ, 653, 462
Guetta, D., & Piran, T. 2005, A&A, 435, 421
Gürsel, Y., & Tinto, M. 1989, Phys. Rev. D, 40, 3884

Hansen, B. M. S., & Lyutikov, M. 2001, MNRAS, 322, 695
Harry, I. W., & Fairhurst, S. 2011, Phys. Rev. D, 83, 084002
Hjorth, J., Watson, D., Fynbo, J. P. U., et al. 2005, Nature, 437, 859
Holz, D. E., & Hughes, S. A. 2005, ApJ, 629, 15
Hughes, S. A., & Holz, D. E. 2003, Class. Quantum Grav., 20, 65
Hurley, K., Boggs, S. E., Smith, D. M., et al. 2005, Nature, 434, 1098
Janka, H.-T., Eberl, T., Ruffert, M., & Fryer, C. L. 1999, ApJ, 527, L39
Kanner, J., Huard, T. L., Márka, S., et al. 2008, Class. Quantum Grav., 25, 184034
Kelley, L. Z., Ramirez-Ruiz, E., Zemp, M., Diemand, J., & Mandel, I. 2010, ApJ, 725, L91
Kochanek, C. S., & Piran, T. 1993, ApJ, 417, L17
Kopparapu, R. K., Hanna, C., Kalogera, V., et al. 2008, ApJ, 675, 1459
Krolak, A., & Schutz, B. F. 1987, Gen. Relativ. Grav., 19, 1163
Kulkarni, S., & Kasliwal, M. M. 2009, in Proc. RIKEN Symp., Astrophysics with All-Sky X-Ray Observations, ed. N. Kawai, T. Mihara, M. Kohama, & M. Suzuki (Saitama: RIKEN), 312
Kulkarni, S. R. 2005, arXiv:astro-ph/0510256
Kulkarni, S. R., Frail, D. A., Wieringa, M. H., et al. 1998, Nature, 395, 663
Kuroda, K., & LCGT Collaboration. 2010, Class. Quantum Grav., 27, 084004
Kyutoku, K., Okawa, H., Shibata, M., & Taniguchi, K. 2011, Phys. Rev. D, 84, 064018
Lattimer, J. M., & Schramm, D. N. 1974, ApJ, 192, L145
Lawler, J. E., Sneden, C., Cowan, J. J., Ivans, I. I., & Den Hartog, E. A. 2009, ApJS, 182, 51
Lee, W. H. 2001, MNRAS, 328, 583
Lee, W. H., Ramirez-Ruiz, E., & López-Cámara, D. 2009, ApJ, 699, L93
Lee, W. H., Ramirez-Ruiz, E., & van de Ven, G. 2010, ApJ, 720, 953
Leibler, C. N., & Berger, E. 2010, ApJ, 725, 1202
Li, L., & Paczyński, B. 1998, ApJ, 507, L59
Lyutikov, M. 2011a, Phys. Rev. D, 83, 124035
Lyutikov, M. 2011b, Phys. Rev. D, 83, 064001
MacFadyen, A. I., Ramirez-Ruiz, E., & Zhang, W. 2005, arXiv: astro-ph/0510192
Mandel, I., & O'Shaughnessy, R. 2010, Class. Quantum Grav., 27, 114007
McWilliams, S. T., & Levin, J. 2011, ApJ, 742, 90
Metzger, B. D., Arcones, A., Quataert, E., & Martínez-Pinedo, G. 2010a, MNRAS, 402, 2771
Metzger, B. D., Martínez-Pinedo, G., Darbha, S., et al. 2010b, MNRAS, 406, 2650
Metzger, B. D., Piro, A. L., & Quataert, E. 2008a, MNRAS, 390, 781
Metzger, B. D., Piro, A. L., & Quataert, E. 2009, MNRAS, 396, 304
Metzger, B. D., Quataert, E., & Thompson, T. A. 2008b, MNRAS, 385, 1455
Mohanty, S. D., Marka, S., Rahkola, R., et al. 2004, Class. Quantum Grav., 21, 765
Nakar, E., Gal-Yam, A., & Fox, D. B. 2006, ApJ, 650, 281
Nakar, E., & Piran, T. 2011, Nature, 478, 82
Nakar, E., & Sari, R. 2010, ApJ, 725, 904
Narayan, R., Paczynski, B., & Piran, T. 1992, ApJ, 395, L83
Nissanke, S., Holz, D. E., Hughes, S. A., Dalal, N., & Sievers, J. L. 2010, ApJ, 725, 496
Nissanke, S. M., Sievers, J. L., Dalal, N., & Holz, D. E. 2011, arXiv e-prints
Norris, J. P., & Bonnell, J. T. 2006, ApJ, 643, 266
Nuttall, L. K., & Sutton, P. J. 2010, Phys. Rev. D, 82, 102002
O'Shaughnessy, R., Belczynski, K., & Kalogera, V. 2008, ApJ, 675, 566
Paczynski, B. 1986, ApJ, 308, L43
Perley, D. A., Metzger, B. D., Granot, J., et al. 2009, ApJ, 696, 1871
Phinney, E. S. 2009, in Astro2010: The Astronomy and Astrophysics Decadal Survey, Science White Papers, 235
Rezzolla, L., Giacomazzo, B., Baiotti, L., et al. 2011, ApJ, 732, L6
Roberts, L. F., Kasen, D., Lee, W. H., & Ramirez-Ruiz, E. 2011, ApJ, 736, L21
Rosswog, S. 2005, ApJ, 634, 1202
Rosswog, S., Liebendörfer, M., Thielemann, F., et al. 1999, A&A, 341, 499
Rosswog, S., & Ramirez-Ruiz, E. 2002, MNRAS, 336, L7
Rosswog, S., Ramirez-Ruiz, E., & Davies, M. B. 2003, MNRAS, 345, 1077
Rowlinson, A., Wiersema, K., Levan, A. J., et al. 2010, MNRAS, 408, 383
Ruffert, M., Janka, H., Takahashi, K., & Schaefer, G. 1997, A&A, 319, 122
Schutz, B. F. 1986, Nature, 323, 310
Schutz, B. F. 2002, in Proc. MPA/ESO/MPE/USM Joint Astron. Conf., Lighthouses of the Universe: The Most Luminous Celestial Objects and Their Use for Cosmology, ed. M. Gilfanov, R. Sunyeav, & E. Churazov (ESO Astrophys. Symp.; Berlin: Springer-Verlag), 207
Schutz, B. F. 2011, Class. Quantum Grav., 28, 125023
Shibata, M., & Taniguchi, K. 2008, Phys. Rev. D, 77, 084015
Sneden, C., Cowan, J. J., Lawler, J. E., et al. 2003, ApJ, 591, 936
Soderberg, A. M., Berger, E., Kasliwal, M., et al. 2006, ApJ, 650, 261
Soderberg, A. M., Chakraborti, S., Pignata, G., et al. 2010, Nature, 463, 513
Stamatikos, M., Gehrels, N., Halzen, F., Mészáros, P., & Roming, P. W. A. 2009, in Astro2010: The Astronomy and Astrophysics Decadal Survey, Science White Papers, 284
Stephens, B. C., East, W. E., & Pretorius, F. 2011, ApJ, 737, L5
Stubbs, C. W. 2008, Class. Quantum Grav., 25, 184033
Sylvestre, J. 2003, ApJ, 591, 1152
The LIGO Scientific Collaboration & Virgo Collaboration 2011, A&A, in press (arXiv:1109.3498)
Troja, E., Rosswog, S., & Gehrels, N. 2010, ApJ, 723, 1711
Tsang, D., Read, J. S., Hinderer, T., Piro, A. L., & Bondarescu, R. 2011, Phys. Rev. Lett., in press (arXiv:1110.0467)
van Eerten, H., Zhang, W., & MacFadyen, A. 2010, ApJ, 722, 235
van Eerten, H. J., & MacFadyen, A. I. 2011, ApJ, 733, L37
Wang, X., Li, W., Filippenko, A. V., et al. 2009, ApJ, 697, 380
Wen, L., & Chen, Y. 2010, Phys. Rev. D, 81, 082001
Yun, M. S., & Carilli, C. L. 2002, ApJ, 568, 88